12-2008

SYNTHESIS, CHARACTERIZATION, AND APPLICATION OF Ag NANOSTRUCTURES

Stephen Hudson
Clemson University, shudson@clemson.edu

SYNTHESIS, CHARACTERIZATION, AND APPLICATION OF Ag NANOSTRUCTURES

A Dissertation
Presented to
the Graduate School of
Clemson University

In Partial Fulfillment
of the Requirements for the Degree
Doctor of Philosophy
Chemistry

---

by
Stephen D. Hudson
December 2008

Accepted by:
George Chumanov, Committee Chair
Kenneth Marcus
Jason McNeill
Igor Luzinov

ABSTRACT

Noble metal nanoparticles (NPs) have been used for many centuries; however their properties were not truly scrutinized until Michael Farady's investigations in the 1850's. Advances in the field of nanotechnology over the last three decades have enabled insights into the properties of materials as their dimensions are reduced to the nanoscale. The repercussions of these insights are seen in many modern applications.

In this dissertation, properties of novel nanostructures based on Ag NPs are presented and discussed. The exceptional optical properties of Ag NPs stem from the collective oscillations of the conduction electrons known as plasmon resonances. The excitation of plasmon resonances leads to the strongest known interaction of light with matter as compared to any known organic or inorganic chromophore.

A novel type of nanostructure, composed of Ag NPs capped with various materials and termed asymmetric hybrid nanoparticles (AHNs) was proposed and implemented. The concept of AHNs allows the addition of new properties to nanoparticles. Metals and dielectric materials were used as caps, imparting strong effects on the plasmon resonances of the AHNs. Multilayer AHNs were fabricated to render magnetic properties to Ag NPs.

The AHN concept led to the development of a novel type of optical labels. The labels are based on the surface enhanced Raman scattering (SERS) phenomenon from organic molecules sandwiched between Ag core and Ag cap. The observed strong SERS is well suited for multiplexed assays with optical detection. The structures were also used for

fundamental SERS investigations. An alternative enhancement mechanism termed plasmon-induced electronic coupling was proposed from the results.

Capitalizing on their large cross-section for the interaction with light, Ag NPs were also investigated as optical labels based on light scattering. Ag NPs were encapsulated in silica shells, modified with amine functionalities, followed by conjugation with neutravidin molecules. Neutravidin offers a scaffold for attaching biotinylated biomolecules including antibodies. Silica shells provided nearly complete protection of Ag core in saline solutions often used in bioanalytical applications. The ongoing work focused on the application of these labels to flow cytometry.

DEDICATION

This work is dedicated to my Lord and Savior, Jesus Christ who has strengthened me through this entire process despite my failures in serving Him. Also, to Grandma Hudson for her ever-cheerful spirit that makes me smile every time I think about her. To my parents, Harold and Laura for raising me to remember that the most important lessons in life are not learned from a textbook. Dad, thank you for setting a godly example before me and encouraging me every step of the way. To my sisters Anna and Sarah for demonstrating such a strong work ethic. You have both worked so hard to achieve your goals and I am proud to have you as my sisters. To Dennis and Connie; thank you for taking in my family as your own. No one has better in-laws than I do, except maybe Sarah. To my beautiful and loving wife, Jessica; I still get chills when I think about how God allowed us to meet. I know I'll never be as good of a husband as you deserve, but I sure will enjoy trying. You have been so understanding and forgiving and I can never repay you except to tell you again how much I love you with all of my heart.

ACKNOWLEDGMENTS

I would like to acknowledge Dr. Pat Owens and all the faculty and staff from the Winthrop University Chemistry department for corralling me into the world of chemistry and giving me opportunities to shine, even when I wasn't very shiny. I would also like to acknowledge my senior group members Dave, Katrina, and Amar for their guidance as well as Dr. Serhiy Malynych for his patience in teaching me how to operate literally everything in the lab. I would like to acknowledge my current group members John and Mark. What a privilege it has been to work with such intelligent minds and great people. Many thanks for all the discussions about plasmonics. And finally, I would like to acknowledge my advisor, Dr. George Chumanov. I never doubted at any point during my graduate career that I had made the right choice about joining this group. The enthusiasm that he has for the science is truly infectious, whether it showed or not. I am grateful for his encouragement and guidance, not only in scientific matters, but in life as well.

AHNs and SSNPs Acknowledgment: This research was supported by the United States Department of Energy, grant No. DE-FG02-06ER46342.

TABLE OF CONTENTS

Page

Table of Contents (Continued)

LIST OF FIGURES

List of Figures (Continued)

CHAPTER ONE

INTRODUCTION

Many interesting phenomena are observed for materials when their dimensions are reduced to the nanometer scale (10 nm – 200 nm). The intriguing characteristics of nanoparticles (NPs) usually originate from their high surface-to-volume ratio, allowing surface-specific properties to dominate the bulk properties normally associated with the material. Noble metals, in particular, are often used in numerous optical applications because of their unique optical properties associated with the excitation of plasmon resonances at the nanoscale. These applications include surface enhanced Raman scattering (SERS)[1-8], surface plasmon waveguides[9-16], optical circuits and devices[17,18], chemical and biological sensing[19-27], cancer detection and therapy[28-31], and photovoltaics.[32-36]

Silver NPs undergo the most efficient interaction with light as compared to any other metal NP, or any known organic or inorganic chromophore.[37] The optical cross-section of Ag NPs is nearly five times that of the same sized Au NPs[38], making them more attractive for optical applications. Although Au NPs have been used for many applications where their resistance to oxidation is the primary consideration, this dissertation will focus on Ag NPs for their favorable optical characteristics.

The unique optical properties of Ag NPs arise from the collective oscillations of conduction electrons excited by the electric vector of incident light interacting with the particle.[39] When the dimensions of the NP are much smaller than the wavelength of the

incident light, the extinction spectrum (the sum of the absorbance and scattering cross sections) *E(λ)* of a spherical metal nanoparticle is described by the equation

$$E(\lambda) \propto \left[\frac{\epsilon_i(\omega)}{[\epsilon_r(\omega) + \chi \epsilon_{med}(\omega)]^2 + \epsilon_i(\omega)^2} \right] \quad (1.1)^{[39]}$$

where $\epsilon_r(\omega)$ and $\epsilon_i(\omega)$ are the real and imaginary parts of the dielectric function of the metal, respectively, $\epsilon_{med}(\omega)$ is the dielectric function of the surrounding medium that creates the local environment, λ is the wavelength of excitation, and χ is a constant that depends on the particle shape and is equal to 2 for spherical particles.[39] Both parts of the complex dielectric function of metals are wavelength dependent and determine how light interacts with the metal. The imaginary part for Ag does not change significantly in the visible spectral range, whereas the real component becomes increasingly negative as the wavelength increases. From equation 1.1 it can be seen that a maximum in the extinction spectrum will be observed for small metal NPs when ϵ_r is equal to $-2\epsilon_{med}$ and $|\epsilon_r| >> \epsilon_i$. When this condition is met, conduction electrons in the NP can be perturbed in a resonant manner at the frequency of the incident light, leading to a collective oscillation of the 'free' electron density known as a plasmon resonance (Figure 1.1). Such collective oscillations in thin metal films are known as surface plasmons (SPs) and, when confined to a 3D nanometer-scale structure, are termed localized surface plasmon resonances (LSPRs). For small (10 – 80 nm) Ag NPs, LSPRs are manifested as a single peak in their extinction spectrum.

An important consideration for metal NPs is that the mean free path of the electrons is larger than the dimensions of the particle, allowing the free electron density to act as a

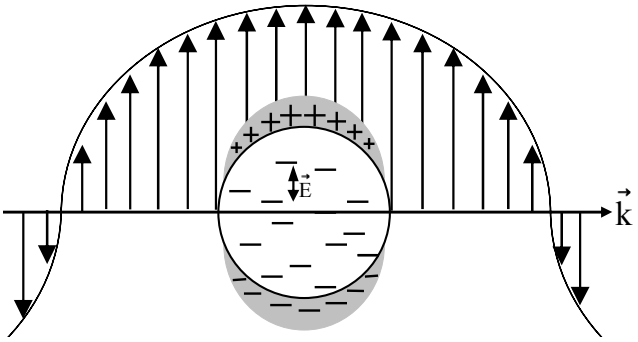

Figure 1.1 Electric vector $\vec{E}$ induces collective oscillations of the 'free' conduction electrons, establishing a charge dipole on the particle as the electron cloud is displaced slightly from the lattice of positively charged nuclei.

cloud of charges, or plasma. The electric vector $\vec{E}$ of incident light forces this cloud to oscillate, thereby slightly redistributing the electron density and inducing a particularly strong dipole moment in the NP (Figure 1.1). This strong dipole moment is a feature associated with the excitation of LSPRs and is responsible for their high optical cross sections as well as the generation of local fields near the particle's surface.[2,37,40-42] The local field is enhanced as compared to the incident field as the result of a redistribution of the incident and scattered electromagnetic fields at the surface of the NP.

The size and shape of the particles plays an important role in determining the spectral width and position of the plasmon resonance.[43-47] The plasmon resonance wavelength for spherical NPs scales with the diameter of the particle, and for Ag NPs, the shape of the extinction band corresponding to the plasmon resonance of Ag NPs remains as a single, nearly symmetric peak until the particle diameter approaches the wavelength of incident light. In this case, the phase of the electric vector of light experiences retardation across the NP, resulting in multipolar oscillations of the electron density. This behavior is manifested as the appearance of a quadrapole, octapole, or

hexadecapole, etc. in addition to the dipole. The contributions of these additional modes increases as the NP dimensions continue to grow.[48,49]

Another important size-dependent property of Ag NPs relates to the frequency dependence of $\epsilon_r(\omega)$ and $\epsilon_i(\omega)$ which determine the scattering and absorbing properties of the NPs, respectively. As mentioned above, $\epsilon_i(\omega)$ remains nearly constant across the visible spectral range whereas the value of $\epsilon_r(\omega)$ grows more negative with increasing wavelength. Larger Ag NPs have a peak plasmon resonance at longer wavelengths where the large, negative value of $\epsilon_r(\omega)$ indicates that light scattering from the NPs is a more efficient process than absorption of light. It is important to emphasize that scattering of light is a dominating process for large Ag NPs as compared to light absorption. This behavior has been verified experimentally in our laboratory by independently measuring scattering and extinction spectra of different sized Ag NP.[37] Briefly, both the Ag NP colloidal sample and the detector were placed inside an integrating sphere wherein the line of sight between the sample and detector was obstructed by a baffle. In this configuration, the amount of light scattered by the sample could be independently measured by the detector and subtracted from the extinction spectrum of the same sample to calculate the amount of light absorbed.

The dependence of the optical properties upon the shape of Ag NPs is the topic of many articles and researchers have developed a number of interesting nanostructures such as prisms[50], shells[51-53], rods[54-56], and crescent moon shapes.[57] Nanoprisms are found to have higher than average electric local field concentrations at their vertices, similar to those found at the thin edges of crescent moon nanoparticles. Nanorods have

their own interesting properties in that they posses two primary plasmon resonances simultaneously, a transverse and a longitudinal mode. The higher frequency, transverse mode, corresponds to electrons oscillating perpendicularly to the long axis of the rod whereas the longitudinal mode is tuned to longer wavelengths of light and is attributed to electrons oscillating along the length of the rod.

Surface plasmons are by nature a surface phenomenon rendering them highly sensitive to changes in their local environment. The enhanced local field produced by the dipolar plasmon resonance is a non-propagating field that decays exponentially from the surface of the particle. It was determined in our laboratory for Ag NPs with diameter 84 $\pm$ 5 nm that the local field extends ca. 40 nm into the surrounding medium[58] and a number of theoretical models are available to predict the local field strength and its distribution in various plasmonic systems.[50, 59] The induced dipole moment in the NP also polarizes the local environment around the particle. High polarizability of the surrounding medium, as determined by its large dielectric function (refractive index), will slow the collective electron oscillations in the NP and shift the plasmon resonance to longer wavelengths. Slight changes of the local refractive index around the NP can cause significant changes to the frequency of the plasmon resonance (e.g. raising the local refractive index leads to red-shifted and more intense plasmon resonance peak in the extinction spectrum of Ag NPs). This dependence upon the local refractive index is the behind sensing techniques base on surface plasmon resonance (SPR).[60, 61]

In addition to size, shape, and local dielectric environment changes, the combination of different materials into hybrid nanoparticle structures can be a useful approach for

rendering novel properties to NPs. Sol-gel chemistry is frequently used to form oxide shells around NPs, introducing desired surface chemical properties and/or protecting the particles in aggressive environments. The latter property of these oxide shells is especially important for Ag NPs in biological applications where high NaCl concentrations (ca. 150 mM) could etch the particles by forming insoluble AgCl. Alloying is another method for fabricating hybrid NPs[53,62]; however, alloyed particles usually lack the desirable optical properties of pure noble metal NPs. Recent examples of core/shell particles illustrate the advantages of combining various materials without forming alloys.[30,63-65] Gold nanoshells formed around magnetic cores were used for magnetic separation and pre-concentration of biological samples *in vitro*.[64, 65] Other core/shell structures formed from small clusters of Ag NPs encapsulated with cross-linked bovine serum albumin (BSA) were modified with antibody receptors and used to label specific proteins in human tissues.[66]

Many interesting applications for NPs require that they be arrangement into complex architectures. Ordered patterns of NPs offer many possibilities for sensors[22-24,27,67,68], optical waveguides[9-13,69,70,88], optoelectronics[17,34,71,72], and spectroscopic applications.[1,19,67,68,73,74] Manually arranging individual NPs can be achieved by a few highly advanced scanning probe techniques[76, 77]; however, these bottom-up fabrication methods are costly and time consuming. A more desirable approach is to rationally design both the NPs and the substrate and then allow the system to self-assemble based on their physical and chemical composition. In order to obtain complex architectures by self-assembly, each basic component, or building block, must have multiple, chemically

distinct sites on its surface by which they can be manipulated. In other words, the self-assembly of complex structures requires building blocks of low symmetry. Properties that have been exploited to direct the self-assembly NP structures include but are not limited to the NP's chemical specificity[44,67,78,79] and magnetic susceptibility.[80, 81]

In Chapter 2, the novel concept of Asymmetric Hybrid Nanoparticles (AHNs) and their fabrication that were developed in our laboratory is described. Silver NPs were synthesized with the hydrogen reduction method, producing pure, single crystal NPs with no extraneous surface species. Using this method, the diameter of the NPs can be tuned from 30 nm up to 300 nm with a narrow size distribution. Immobilization of these particles on glass substrates followed by the deposition various materials allowed them to be coated with hemispherical caps of via physical vapor deposition. The particles could then be stripped from the substrate and used as individual NPs. This fabrication technique is advantageous because it renders new properties to the NPs while maintaining their desirable optical characteristics. The reproducibility of this method is high as each particle is capped with the same amount of material. By modifying only one half of each particle, the symmetry of the building blocks is lowered. Various materials were used for caps and each material was investigated to determine new properties of the Ag AHNs. This work was published in *Chemistry of Materials* (Copyright 2007 American Chemical Society). The citation for this manuscript is:

S. D. Hudson, G. Chumanov, Synthesis and Characterization of Plasmonic Asymmetric Hybrid Nanoparticles, *Chem. Mater.* **2007**, 19, 4222 – 4227.

Surface enhanced Raman scattering[6] has been established as a powerful analytical technique over the last three decades. The growth and rapid development of SERS relates to the wealth of vibrational information it provides without many of the restrictions inherent to IR vibrational spectroscopy. Raman spectra are not inhibited by the presence of water and can be measured across most of the visible and near-IR spectral range. SERS originates from molecules that are in close proximity to nanostructured metal surfaces, primarily silver and gold, capable of supporting plasmon resonances in the visible spectral region where Raman scattering is excited. The phenomenon provides the basis for a powerful analytical technique offering both quantitative and qualitative molecular information about biological molecules.[42] Contrary to IR spectroscopy, the Raman scattering cross section of water molecules is small, allowing vibrational information to be obtained from biological molecules in their native aqueous environment and their efficient detection and discrimination from the background. Low detection limits, narrow spectral bandwidths, the ability to quench fluorescence, and the possibility to be used with or without optical labels, make SERS a good choice for DNA or RNA analysis[136-138], genetics and proteomics[139], medical diagnostics[23,140], and the detection of chemical warfare agents.[23,27,141]

The enhancement of Raman scattering and, ultimately, the sensitivity and low detection limits potentially attainable from SERS strongly depend upon the nanoscale surface morphology of the enhancing surfaces, making reproducible and quantitative measurements difficult. Numerous efforts focused on quantifying and controlling this dependence have led to the development of a variety of rationally designed SERS

substrates, a topic that has been recently reviewed by Mirkin *et al.*[142] The review highlights progress from their own group towards the development of so-called "on-wire lithography" wherein electrochemical deposition is used for the fabrication of alternating layers of Ni and Au in the pores of an aluminum oxide template. The resultant layers of ~30 nm Ni between 120 nm thick Au disks provided novel nanostructures with tunable SERS response and were applied to the multiplexed analysis of oligonucleotides with a limit of detection (LOD) of ~ 100 fM. Other work by Talley and co-workers illustrated the use of ~30 nm hollow gold nanospheres for quantitative pH analysis with a resolution of 0.5 pH units over a range of from pH 3.5 to pH 9.[51] Vo-Dinh *et al.* also demonstrated a promising new development of "molecular sentinel nanoprobes" wherein Ag nanoparticles (Ag NPs) modified with single-stranded DNA (ssDNA) labeled with a Raman reporter were used to detect single molecules of complimentary ssDNA from breast cancer cells.[138] Mirror sandwich SERS substrates (M3S) developed in our laboratory were composed of monolayers of Ag NPs attached onto Ag mirror films using polymers that exhibit affinity to silver [19, 20], as illustrated in Figure 1.2. Plasmon coupling between the NPs as well as between NPs and the Ag mirror resulted in reproducible substrates producing strong SERS. These substrates were used to monitor the germination kinetics of *Bacillus subtilis* spores, a well-known analogue for the anthrax virus [19], and detection limits down to a single spore were achieved.[20] Silver NPs reduced with EDTA were applied for the quantitative SERS measurements of folic acid in aqueous and serum solutions in the concentration range between 18 nM and 1uM.[143] Hernandez-Rivera *et al.* performed optimization studies for sodium citrate and

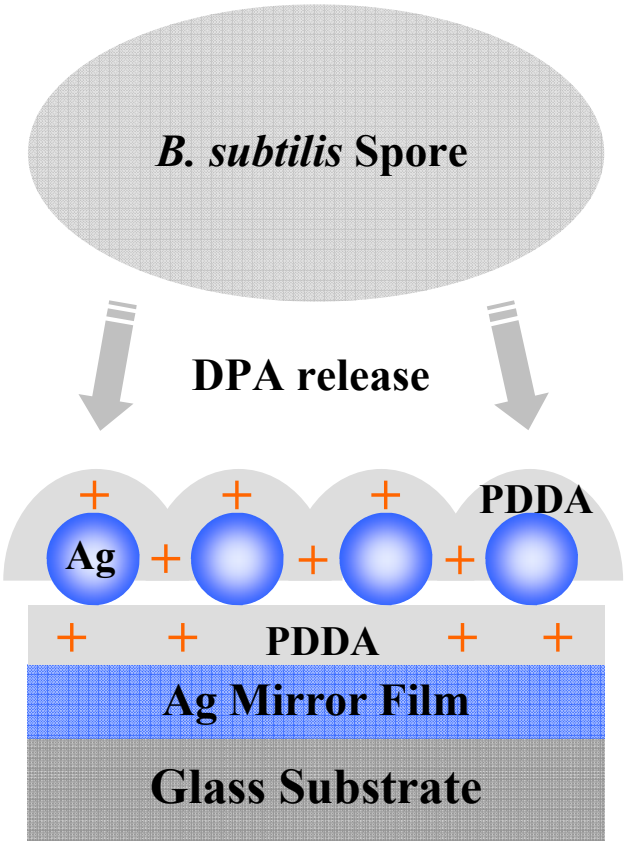

Figure 1.2 Schematic of an M3S SERS substrate with an adsorbed spore

hydroxylamine hydrochloride reduction of Ag colloids and synthesized Au, Ag/Ag, and Au/Ag alloyed colloidal suspensions for detection and discrimination of dinitrotoluene (DNT) and trinitrotoluene (TNT) as well as different bacterial species.[23]

New developments towards sampling techniques based on microchannel flow-cells have also proven to be successful for quantitative SERS measurements. Chaotic mixing inside the microchannels provided an ensemble-averaged scattering signal that obviated spot-to-spot intensity fluctuations commonly observed with static SERS measurements. Microfluidic flow cells made of polydimethylsiloxane (PDMS) in an 'alligator teeth' shape design have been developed by Lee and co-workers and used to quantitatively

measure methyl parathion pesticides with an LOD of 0.1 ppm.[144] Real-time quantitative detection of RNA bases via flow-injection analysis was achieved by Ni *et al.* [137], and 4 x 10^{-11} M concentrations of mitoxantrone (an anticancer drug) have also been detected with RMS precision of $\leq$ 5% in aqueous and biological solutions.[145] Coté and co-workers illustrated a novel 'micro-to-nanochannel' device consisting of a 40 nm channel in the middle of a microchannel to trap and aggregate 60 nm Au NPs.[139] The conformation-dependent SERS spectra of β-amyloid proteins was measured on the NP aggregates, thereby demonstrating the potential of this approach for early detection of Alzheimer's disease. A recent review of SERS combined with microfluidic methods has been published by Chen and Choo.[146]

An ideal SERS substrate should be easily fabricated yet reproducible and simple enough for integration into analytical devices that can be operated by non-experts in the field. Electron beam lithography (EBL) techniques can provide precise control over surface topography; however, EBL is costly and is limited to small pattern areas that are not practical for many end-use analytical applications. Recent developments have resulted in substrates with large areas patterned on the nanoscale, as demonstrated in the pioneering work of Van Duyne *et al.*, wherein a tightly packed array of sub-micron silica or polymer beads was used as a template for thermal vapor deposition of Au or Ag patterns on the underlying substrate.[147] The technique was termed nanosphere lithography (NSL) and provided control of the nanoscale morphology on the macroscale in a simple, cost effective manner. The substrates were used for the detection of biochemical markers for Alzheimer's disease[148] as well as in a number of fundamental

studies of the SERS phenomenon.[149] In a different modification of this technique, termed Ag film-over-nanospheres (AgFON), a thin Ag film was deposited onto the array of submicron spheres, and was used for *in vivo* glucose sensing.[25] The AgFONs, and a different AgNP substrate developed by Vo-Dinh *et al.* were both successfully incorporated into real-world portable analysis instruments for field use for detection of biological warfare agents.[27, 150] Abdelsalam and co-workers used colloidal templates to produce Ag patterns of inverse hexagonal arrays for electrochemical SERS detection of a flavin analogue with sub-femtomolar LODs.[151] Tripp *et al.* have developed a novel SERS substrate based on oblique angle deposition (OAD) of silver resulting in tightly packed arrays of nanorods that provided excellent detection limits for viruses with enhancement factors of greater than 10^8 and analysis times of less than 1 minute.[68] These substrates were further used to discriminate between various strains of viruses and to determine different gene deletions within the same strain of virus.

Advances in instrumentation and detection schemes have led to significant improvements in quantitative SERS measurements. Confocal Raman microscopy is a powerful technique that allows high spatial resolution in both the x-y plane and z axis and has been applied to many SERS experiments described in this article. Surface enhanced resonance Raman scattering (SERRS) is gaining more attention for achieving larger enhancement factors from molecules containing chromophores with an optical transition at or near the frequency of the excitation source.[152] Internal standards such as CNS^- are also becoming a prevalent tool for quantitative SERS analyses and can account for variations of the signal intensity due to excitation source fluctuations and differences in

alignment.[153] Another sampling method, termed the multiple points collection technique, was developed by Zenobi and co-workers to reduce signal variations from substrate irregularities and decrease carbon deposits from sample overheating.[154] This technique uses galvanic mirrors to scan the laser source across the sample, creating an averaged signal for each spectrum, thereby reducing sample heating and yielding quantitative, ensemble-averaged spectra for cytochrome C, immunoglobulin M, and dipicolinic acid (DPA) which is a common marker for bacteria spores in the genus *Bacillus*.

New protocols for sample preparation have also resulted in better detection limits and increased signal reproducibility. A new protocol for the preparation of DNA samples was developed by Halas *et al.* to yield highly reproducible SERS spectra from ssDNA and double stranded DNA (dsDNA).[136] Investigations on non-pretreated DNA reported significant variations of the SERS signal measured from different areas of the same substrate as well as from different substrates containing the same ssDNA and dsDNA molecules.[136] These variations were attributed to the random coiling of DNA oligomers. Their new protocol employed a non-destructive thermal pretreatment followed by a rapid cooling cycle which relaxed the random coiling of DNA and allowed the oligomers to adopt a more linear conformation. Following adsorption to Au nanoshells via a thiol group, SERS measurements demonstrated remarkable improvement in signal reproducibility as compared to non-pretreated DNA.

Optical labeling has become a standard technique for the detection of biomarkers in biological samples such as tissues and individual cells.[3,153] SERS optical labels provide

robust labeling capabilities with higher spectral resolution as compared to fluorescent dyes, allowing more target species to be labeled within a given window of frequencies. The most commonly used approach is based on extrinsic labeling that utilizes synthetic markers such as fluorescent dyes or other Raman-active molecules with a large scattering cross-section. The markers are called Raman reporters and are attached to SERS-active nanoparticles together with molecules capable of recognizing the target analyte. An example of this approach was demonstrated with composite organic – inorganic nanoparticles (COINs)[66], the synthesis of which is depicted in Figure 1.3. COINs were composed of Ag NPs aggregated in the presence of Raman reporter molecules that become trapped between the NPs. The aggregates were encapsulated in bovine serum albumin cross-linked with glutaraldahyde to form a protective, organic shell around the cluster that was subsequently conjugated with antigens or antibodies as recognition molecules. The COINs with two different Raman reporters were applied for the detection of prostate specific antigen (PSA) in *in vitro* tissue samples (Figure 1.4) and demonstrated highly sensitive and specific multiplexed response. Similarly, Au nanorods capped with hexadecyl-trimethylammonium bromide (CTAB) and coated with (poly)styrenesulfonate produced strong, anisotropic SERS signals from cancer cells.[54] Adsorption of the nanorods to specific constituents on the cell walls led to alignment of the rods and, consequently, a strongly polarized SERS signal. Another example of extrinsic labeling for multiplexed SERS imaging was demonstrated by the Gambhir laboratory where Nanoplex Biotags (Oxonica) and single-walled carbon nanotubes were used for whole-body deep-tissue imaging on a live mouse.[156] Image internal organs (i.e.

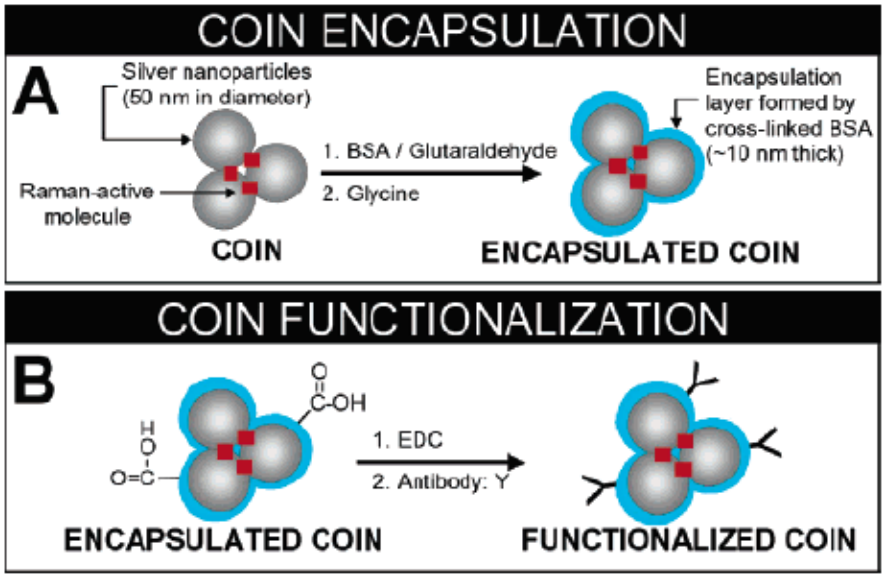

Figure 1.3 COIN encapsulation and functionalization method. (A) Schematic illustration of COIN encapsulation procedure. Bovine serum albumin (BSA) is coated to the COIN surface and crosslinked by glutaraldehyde. The extra aldehyde functional groups on the COIN surface are removed by glycine and sodium borohydride treatment. (B) Schematic illustration of COIN functionalization procedure. Carboxylic acid groups on the surface of the BSA encapsulation layer are activated by EDC and reacted with amines groups in the antibody. (Adapted from reference 66).

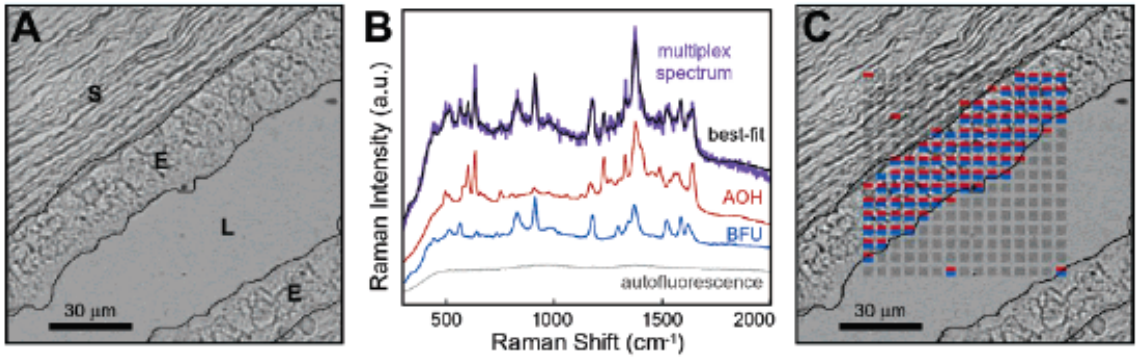

Figure 1.4 Simultaneous two-COIN staining for PSA antigen. (A) Brightfield tissue image showing stroma (S), epithelium (E), and lumen (L). (B) Spectral fitting in duplex COIN experiments on tissue. The upper set of spectra are the measured spectrum from a single point in the epithelium (purple) and the best-fit spectrum (black) found from least-squares regression using reference spectra. The major fitting components are the two conjugated COIN (red, AOH-AbPSA; blue, BFU-AbPSA) and the tissue autofluorescence (gray). The measured spectrum (purple) was acquired in 0.1 s. (C) PSA expression patterns reported by two COINs in a simultaneous duplex measurement. In each pixel, color represents PSA-positive classification based on BFU-AbPSA (blue) and AOH-AbPSA (red), and gray represents PSA-negative classification. Both COINs report PSA-positive expression for nearly every point in the epithelium (i.e., pixels with red and blue). (Adapted from ref. 66)

collect other protein-labeled Au NPs *in situ*, followed by their magnetic separation and liver) as well as subcutaneous tumors were obtained using near infrared (NIR) excitation and scanning confocal microscopy.

Another bioanalytical SERS technique that is becoming popular was illustrated by Lim *et al.* in which magnetic NP cores were coated with bio-functionalized Au shells. These NPs were used for *in vitro* and *in vivo* detection via surface plasmon resonance and SERS and magnetic separation of target species.[65] In order to demonstrate the utility of this technique, the magnetic/Au NPs were functionalized with antibodies and used topre-concentration for further detection with SERS.

Capped, single Ag NPs developed in our laboratory demonstrated a novel and facile method for synthesizing strongly scattering, single NP optical labels for potential bioanalytical applications.[5] Silver NPs modified with Raman reporter molecules were further capped with a thin Ag film to simulate aggregates, specifically dimers, known to produce strong SERS for molecules trapped between the particles. These capped labels yielded strong and stable SERS signals from Raman reporters such as 4-mercaptobenzoic acid, 4-aminothiophenol, and adenine with the signal-to-noise ratio as high as ca. 100 from a single NP, 10 μW of excitation power, and one second accumulation time.

Current efforts are also being focused on measuring SERS from native chemical components in biological samples in an attempt to circumvent the necessity of external labels, a technique termed 'intrinsic labeling'. The presence of Raman-active molecules in biological tissues along with their specific spectral 'fingerprint' potentially enables many biological components to be discriminated without the need for additional sample

manipulation. Living cells incubated with 60 nm Au NPs were shown to incorporate the NPs via fluid-phase uptake and subsequent SERS analysis provided a 'map' of different Raman-active constituents at different locations in the cell.[87] In a related study, Tang *et al.* combined both intrinsic and extrinsic labeling techniques to study intracellular components by introducing non-labeled and rhodamine 6G-labeled Au NPs to live human cancer cells.[157] The Adar research group developed a more complex detection scheme based on a technique termed multispectral imaging whereby both fluorescence and SERRS spectra of the same anti-cancer drug (mitoxantrone) were collected simultaneously inside a single cell.[158] An overlay of the spectral maps with bright-field images of the cell yielded valuable information about local concentrations of the mitoxantrone.

SERS-based immunoassays are currently being developed taking advantage of narrow spectral widths from Raman reporters, reduced bleaching, and the possibility of using NIR wavelengths for detection. A sandwich immunoassay developed by Huan and Yu[159] used close-packed arrays of Au NPs (ca. 47 nm diameter) and crystal violet molecules entrapped inside antibody-modified liposome particles as labels to measure human immunoglobulin G (IgG) with a detection limit of 8 ng/mL. Guo and Wang have also demonstrated peptide-capped Au nanoparticles with subsequent Ag deposition for peptide, peptide-protein, and protein-antibody interaction assays.[160] Their method employed microarrays and IgG/protein A and biotin/avidin recognition pairs for the detection of surface bound and solution based proteins. In a recent review of SERS bioassay methodologies, Porter and co-workers described SERS detection of a single

analyte in a sandwich immunoassay configuration by placing the analyte molecule between an Au substrate and an Au NP labeled with Raman reporters.[155] The review also discusses the role of plasmon coupling between the substrate and the Raman label. Interest in the application of SERRS to immunoassays has also grown because of the potential to simultaneously measure more labels with sensitivity comparable to that obtained with fluorescence methods, as was examined in a recent work by Smith *et al.*[161] Benefits of SERRS-based immunoassays were also combined with the pretreatment procedures used in enzyme-linked immunoabsorbent assays (ELISA) to measure binding between human IgG and anti-IgG labeled with fluorescein isothiocyanate.[162] SERRS allowed concentration measurements without the necessity of carrying out the enzymatic reaction. Simple detection directly from the bottom of a microtiter plate resulted in a LOD of 0.2 ng/mL. SERRS was also incorporated into a bead-based, lab-on-a-chip immunoassay for the detection of *Chlamydia,* offering both the advantages of being rapid and requiring small sample volumes as compared to traditional detection methods.[163]

As SERS investigations become increasingly focused on smaller dimensions, the ability to manipulate plasmonic nanostructures receives a higher priority, especially in light of the highly sensitive nature of the enhancement effect as a function of the proximity of molecules to the substrate surface. Using sharp metal tips (diameter ~10 nm) that act as individual plasmonic nanostructures, atomic force microscopy and confocal microscopy can be used to acquire SERS spectra with lateral and vertical resolutions on the order of tens of nanometers. The spatial resolution afforded by this technique allows researchers to precisely control the interaction of sample molecules with

the enhanced electric field produced by the plasmonic tip, thereby providing useful fundamental information about the surface enhancement process. TERS also offers the unique ability to attain enhanced Raman signals and topographical information simultaneously, and was applied to bacterial cells [164], individual proteins [165], DNA[166], and even single RNA bases.[166,167] In principle, the TERS technique could be used to perform direct, label-free sequencing of DNA which could significantly reduce analysis time and sample size requirements from that of current detection methods. Zenobi and co-workers demonstrated that TERS can be used to discriminate complex biological macromolecules, such as alginate biofilms that have utility for bioengineering coatings and drug delivery systems.[168] Investigations of cytochrome C[165] revealed that Raman spectra from different areas of bio-macromolecules measured with TERS can be significantly different from those obtained with bulk Raman measurements of the sample, further emphasizing the importance of understanding near-field SERS principles. TERS can provide signal-to-noise ratios of $10^4 - 10^5$ due to the highly localized nature of the probe, and Raman enhancement factors up to 10^6 have been achieved.[169] Current challenges for this technique are to gain more precise control over the tip morphology as well as to improve optics and data collection methods.

The ability to quickly differentiate various species of bacteria and viruses is important to medical diagnostics and for the detection of biological warfare agents. Many currently used biochemical methods of analysis are limited by the time required to grow cell or bacterial cultures. SERS provides a novel technology for rapid, non-destructive detection and discrimination of bacteria and viruses at the strain level with minimal sample

preparation. Multivariate analysis can be used to discriminate subtle differences between complicated SERS spectra of specific biomolecules or the 'whole organism' such as a bacteria or virus.[140] Tripp and co-workers, were able to unambiguously identify respiratory syncytial virus (RSV), human immunodeficiency virus (HIV), rotovirus, and the bacterium *M. pneumoniae* in only 30 seconds from a 1 μL sample volume using the OAD substrates as described above.[68] They incorporated principle component analysis (PCA) and hierarchical cluster analysis (HCA), two common multivariate analytical techniques that both provided 100% accuracy for the identification of each sample. Similarly, principle component-discriminant function analysis (PC-DFA) was used discriminate gram positive and gram negative bacteria [170], demonstrating that bacteria with similar outer membrane compositions could be differentiated by their SERS spectra alone. Further work by Hernandez-Rivera *et al.* employed PCA, DFA, and HCA to correctly identify eleven different bacterial species with minimal sample preparation.[23] Pearman *et al.* employed PCA and HCA analyses to detect chemical and biological warfare simulants on Au colloid-based SERS substrates.[141] The ultimate goal is the development of a spectral database that, together with multivariate analysis, enables the identification of unknown samples. The standardization of experimental procedures for measuring SERS spectra from various samples is a prerequisite for the successful application of this database. This standardization could prove difficult considering the vast number of different techniques and substrates for available SERS measurements.

The unique ability of SERS to provide molecular vibrational information with sensitivity down to single molecules in biologically relevant media offers a powerful

analytical system that is ideally suited for *in vitro* and *in vivo* applications. More precise control of rationally designed substrates will allow SERS to become a standard quantitative technique in more bioanalytical applications. The combination of SERS and multivariate analysis will progress to result in methods for rapid medical diagnostics of infectious diseases including lab-on-a-chip with portable SERS instrumentation for point-of-care applications. The development of searchable databases of SERS spectra as well as standard operating procedures for SERS measurements should be a high priority. Although TERS techniques are often costly, they have potential to yield unique information about fundamental aspects of the SERS phenomenon itself as well as lead to the development of label free analysis of individual biomolecules. Sequencing of DNA seems to be a good candidate for such development however improvement of sample preparation methods and better control of the tip morphology are necessary before this and other single molecule applications can be performed on a routine basis. Surface enhanced Raman scattering is truly an up-and-coming contender as the premier analytical technique for biological and biochemical studies in the 21st century.

SERS is also becoming a favored technique for many applications that traditionally have been based on fluorescence spectroscopy, such as optical labeling. This influx of SERS-based labeling methods is primarily due to the lack of photobleaching and the narrow bandwidths of Raman spectral features, leading to the possibility to perform multispectral analyses. High optical cross-sections in the visible and near IR spectral ranges and the ability to produce enhanced local field makes Ag NPs ideally suited for SERS. Raman scattering is a rare event produced by approximately 1 out every 10^7

photons incident on a Raman-active molecule when it undergoes a vibration that changes the polarizability of the molecule. In the presence of highly concentrated electromagnetic fields, such as enhanced local fields produced near the surface of plasmonic NPs, the number of photons incident on a molecule is increased and the number of Raman scattering events increases accordingly. This electromagnetic mechanism (EM) is credited with SERS enhancement factors on the order of 10^{11} – 10^{12} in many studies.[2,57,67,82-87,110] Raman-active molecules that have specific interactions with the metal NP surface can also benefit from a larger change in their polarizability, leading to another 2 – 3 orders of enhancement in their Raman scattering intensity according the chemical enhancement mechanism (CM).[88,89] Additionally, some molecules can form charge-transfer complexes with the NPs wherein an electron is either donated or received by the molecule and resulting in a new resonant complex.

The SERS effect was observed in 1974 by Fleischman[90] and further confirmed and explained in 1977 by Creighton[91] and independently by Van Duyne.[92] Since that time, progress in the field of nanotechnology has allowed researchers to gain greater control over synthetic methods for precise nanostructures and has led to a more thorough understanding of plasmon physics and its role in surface enhancement effects. Two basic prerequisites for producing strong SERS can be identified from these previous works: the excitation of plasmon resonances and a strong interaction between the molecule and the metal surface.

A recent SERS study in our laboratory was performed on 2D coupled Ag NP arrays immobilized on Ag mirror substrates. The SERS from 20 different molecules was

studied; however, the results could not be completely explained with the EM and CM.[75] Another model, termed the *plasmon-induced electronic coupling* (*PIEC*) mechanism, was introduced to explain the experimental results. It was proposed that the oscillating conduction electrons associated with the excitation of plasmon resonance in the Ag NPs penetrate into the electronic system of adsorbed molecules. As a result, these conduction electrons become modulated with the vibrational frequencies of the molecule, and upon returning to the NP, scatter Raman-shifted frequencies.

A novel SERS system is introduced in Chapter 3 based on capped single Ag NPs and provides further evidence for the PIEC model. Individual Ag NPs were modified with different Raman-active molecules and additionally covered with a thin Ag cap. The molecules were sandwiched between the Ag core and cap in this configuration. The Ag cap was separated from the Ag core by only a monolayer of molecules and was considered to be in electrical contact with the core due to the overlap of their electronic wavefunctions. Basic electrodynamics states that the electromagnetic field inside a closed conducting sphere must be equal to 0. Since this is the case, the molecules inside of an Ag NP should not experience any contributions to their SERS via the electromagnetic mechanism. Nevertheless, a strong SERS signal was observed from single capped Ag NPs relative to uncapped NPs, providing evidence for the PIEC mechanism. These particles also form the basis for a new type of optical labels. The work discussed in Chapter 3 was accepted for publication in *The Journal of Physical Chemistry: B.*

The ability to rapidly identify and separate various biological species is a high priority for bioanalytical chemistry and biochemical research as a whole. Optical labeling of molecules is an attractive approach for speciation of biological samples because light-based analytical measurements are the least invasive interrogation methods. A specific application of optical labeling that has significant impact for bioanalytical chemistry is the separation of cells by flow cytometry (FC).[93] With this method, a solution containing fluorescently-labeled cells is focused hydrodynamically into a vertical stream and further broken into individual droplets that presumably contain only a single cell. The droplets pass a laser excitation source and, depending upon their fluorescence signal, can be deflected electrostatically into separate containers for collection.[93,94] Flow cytometry permits cell sorting at a rate of >10,000 cells per second with the use of a number of fluorescent labels.[95] However, because each droplet spends only a short time in the excitation space (ca. 10^{-4} sec.), high loading of the fluorescent labels and high excitation power are necessary to collect sufficient fluorescence signals. High loading of the labels also implies that the cells under investigation must have a commensurate number of chemically specific receptors. Considering that some receptors are only expressed in a few copies and consequently only a few labels can be attached, the individual labels should produce strong signals to compensate for the small number of labels.

Ag NPs provide a suitable alternative to fluorescent labels due to their strong interaction with light, specifically their high scattering efficiency. An important consequence of this strong scattering component is that only a single NP is necessary to

produce a sufficient signal, obviating the requirement for the cell to have multiple receptors. The ability to use only a small number of receptors (or even a single receptor) for labeling of cells will permit cell sorting based on the presence of "rare" receptors (i.e. those that are expressed in a small number of copies). The strength of the scattering from Ag NPs also allows for lower power excitation, therefore inducing less damage to the cells. Chapter 4 introduces a collaborative project for the development of a labeling method for cell sorting FC based on the strong light scattering from Ag NPs. An experimental procedure for labeling cells with the NPs is presented and preliminary results are discussed.

CHAPTER TWO

SYNTHESIS AND CHARACTERIZATION OF PLASMONIC ASYMMETRIC HYBRID NANOPARTICLES

Introduction

Asymmetric Hybrid Nanoparticles (AHNs) consist of a core with one or several caps of different materials deposited on its surface.[52,57,96-103] Contrary to core-shell nanoparticles, the caps of AHNs cover only a part of the core surface resulting in nanostructures that exhibit not only combined properties of both the core and caps but also have asymmetry of chemical and physical properties. The latter attribute renders AHNs capable of directional self-assembly leading to complex architectures not achievable with completely symmetric building blocks.

Physical vapor deposition[102] provides a facile method for fabricating AHNs of various compositions by evaporating different materials on nanoparticles immobilized on solid substrates. Several groups have demonstrated this technique using glass or polystyrene beads as the solid support for asymmetric caps of Au[52,57,96-99], Pt, Pd[52], Ni[97], Ag, Cu, Cr[96], and Al.[96,100] In these studies, glass or polymer beads were spin-coated onto substrates and physical vapor deposition was carried out to deposit the metal cap on the exposed side of the beads. The beads, however, served only as templates for the caps and were discarded or dissolved after deposition. This approach was used to add anisotropic magnetic properties to fluorescent polymer beads and the rotation of the beads was controlled by an external magnetic field.[100] The deposited magnetic cap on the beads was thicker than the skin depth for light at both the excitation and emission

wavelengths of the fluorescence therefore blocking any transmission of light through that side of the particles. As the magnetic field is modulated, all the beads rotate in unison and the fluorescence signal is only emitted in one direction at a time. This leads to a controllable "blinking" of the fluorescence signal increasing the S/N ratio of the measurements.

Other groups have developed synthetic methods for creating metal/semiconductor asymmetric particles in situ resulting in gold caps on CdSe nanocrystals.[103,104] In this two-part synthesis, CdSe nanocrystals were formed via pyrolysis and then a gold cap was chemically deposited onto one or both ends of the nanocrystals. The authors proposed that the gold caps could be useful for integration into wiring and for self-assembly although no specific applications were provided.

Here, the fabrication of novel types of AHNs via thermal evaporation of different materials onto plasmonic Ag nanoparticles is described. We emphasize the extraordinary optical properties of these nanoparticles that result from the excitation of plasmon resonances as well as the ability to change these properties and to add new features by depositing on their surface caps of different materials. The silver core was not only used as a template supporting the caps but became an integral component of the asymmetric nanostructure. These particles are termed plasmonic AHNs. Combined physical, chemical, and optical properties of both the cap and the core materials results in nanoparticles for a variety of applications that are not accessible when unmodified, core/shell, other previously described asymmetric nanoparticles are used. The main goal of the initial studies reported here is to demonstrate the feasibility for synthesizing

plasmonic AHNs and to determine how different materials (both metals and non-metals) affect their plasmon resonances. Using this approach, Ag plasmonic AHNs were synthesized with magnetic properties while simultaneously retaining strong plasmon resonances. Several layers of different materials were also applied to the same Ag NPs thereby producing multilayered plasmonic AHNs. Similarly to hemispherical "caps" deposited on silica spheres that were used to orient and re-immobilize nanoparticles onto substrates[97], plasmonic AHNs with magnetic caps were also vectorially oriented on the substrates using uniform magnetic field.

Experimental Section

Chemicals: Ag2O (99.99%), Cr (99.99%), Ag (99.999%), and optical grade LiF (99.5%) were purchased from Alfa Aesar. Reagent alcohol (Ethyl alcohol) was purchased from Aaper Alcohol and Chemical Company. Fe pellets (99.95%), Ti pellets (99.995%), Ni pellets (99.995%), Al pellets (99.999%), SiO (99.99%) were purchased from Kurt J. Lesker Company. HF (49%) and HNO3 were purchased from Fischer Scientific. Poly(4-vinylpyridine) (PVP), 160,000 MW, was purchased from Aldrich. All chemicals were used as received. Ultra-pure water with 18MΩ·cm resistivity was obtained from a standard four-bowl Millipure Milli-Q water purification system.

Methods: Particles were prepared as described in [105], filtered four times and used without centrifugation or concentrating. Post modification centrifugation was done using a Fisher Scientific Centrific Model 228. Extinction spectra were obtained using a Shimadzu UV-2501PC spectrometer. All spectra were processed and figures prepared

using Spectra-Solve for Windows (LasTek Pty. Ltd.). Particle dimensions were measured and XPS spectra were acquired with a Hitachi HD-2000 STEM operating at 200 keV. Formvar-coated copper TEM grids with type B carbon were purchased from Ted Pella, Inc.

Results and Discussion

Single crystal, Ag NPs with characteristic dimension of ca. 90 ± 5 nm were synthesized via the hydrogen reduction method[105]. The resultant bare particles did not have any extraneous chemicals adsorbed on their surface except silver oxide/hydroxide species that are not known to interfere with any surface chemistry. Surface silver oxide and hydroxide stabilize the particles in aqueous suspensions by preventing their aggregation. The absence of extraneous species on the surface of these Ag NPs is an important feature that provides the flexibility for surface modification to tailor the adhesion properties of the core surface to the caps from a variety of different materials. The UV-Vis extinction spectra of ca. 90 nm Ag NPs in water are characterized by the presence of an intense broad band at 490 nm due to the dipolar component and a much weaker band at 418 nm that appears on the side of the broad band due to the quadrupolar component of the plasmon resonances.[37]

Silver NPs were self-assembled from aqueous suspensions on the surface of standard microscope slides modified with PVP. It was previously demonstrated that PVP is a universal surface modifier that can be used for the efficient immobilization of many different nanoparticles on various dielectric and metal substrates.[106] The modified slides

were exposed to a suspension of Ag NPs in deionized water at low ionic strength. Low ionic strength is required in order to maintain long-range electrostatic repulsion between particles and, consequently, for the formation of the assemblies in which particles do not touch each other and do not form 2D aggregates. By changing the exposure time, different density of particles on the slides can be obtained. Care also was exercised to minimize the aggregation of the particles as the slides were dried before placing into a vacuum chamber. This surface aggregation was caused by the capillary forces that developed when solvent evaporated and further supported by the fact that the Ag NPs can freely move on the slide surface uniformly coated with PVP. Consequently, drying of the slides from solvents with smaller surface tension (e. g. alcohol) as well as blocking with metal ions the remaining pyridyl groups of PVP minimized the surface aggregation. After the self-assembly of Ag NPs, their surface can be additionally modified prior to the deposition of the caps. PVP and some other polymers were tested as the surface modifiers however there was no need to do any surface modification of the particles for the plasmonic AHNs reported here. It appeared that all caps adhered to the bare Ag surface sufficiently strong to withstand 15 min sonication in a standard ultrasonic bath. A mild, a few minutes sonication step was used to strip off the plasmonic AHNs from the slides into water or any other suitable solvent that may contain additional molecules to stabilize the plasmonic AHNs or to further modify their surface. It also was concluded that the sonication does not destroy the PVP layer on the slides and the stripped plasmonic AHNs do not carry the PVP molecules on their exposed (not covered with the caps) surface. After the sonication, the slides retained their ability to adsorb Ag

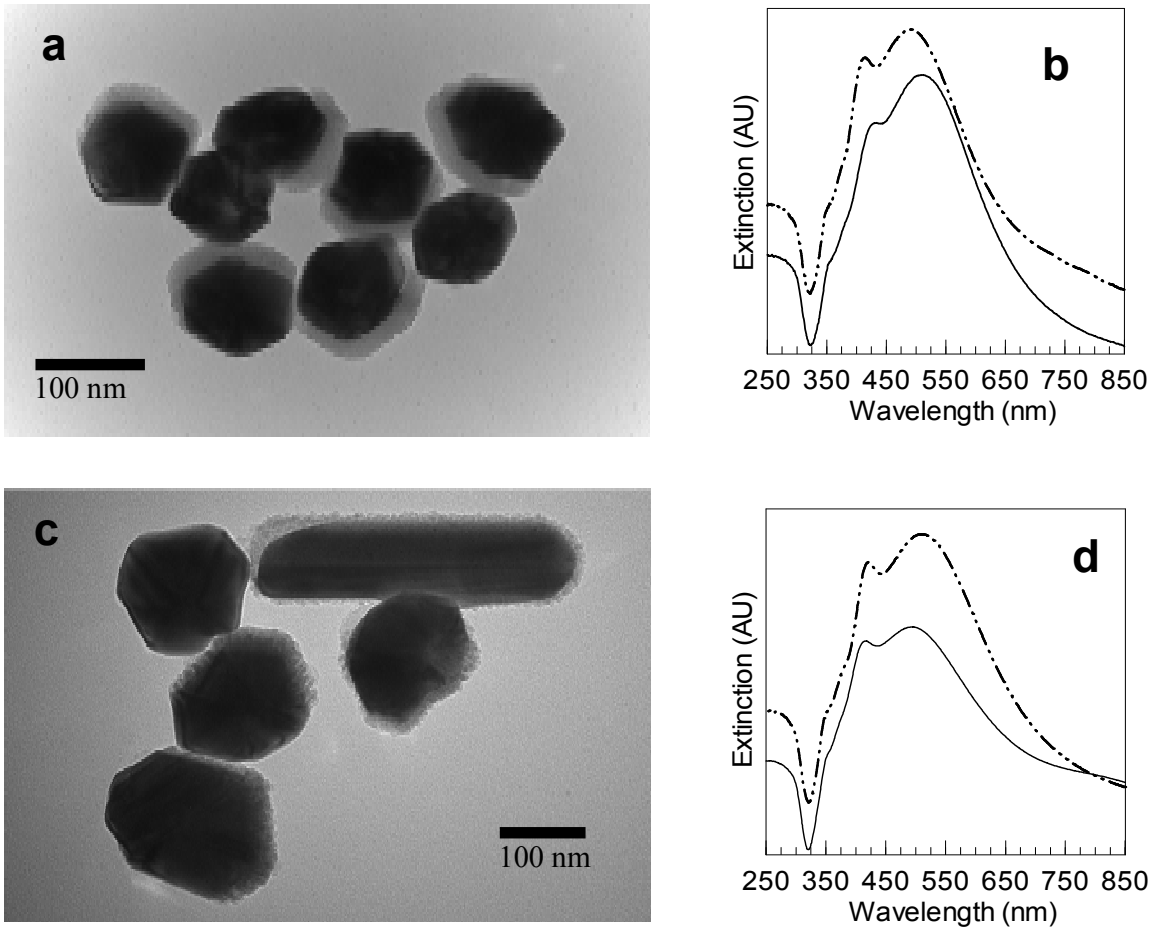

Figure 2.1 TEM (a,c) and UV-Vis spectra (b, d) of plasmonic AHNs with 20 nm silica (a, b) and 10 nm LiF (c, d) caps. Solid curves correspond to plasmonic AHNs and the dashed curves correspond to the same particles without the caps. UV-Vis measurements were performed on stripped particles in water. The spectra in (b, d) are shifted vertically for clarity.

NPs when exposed to the particle suspension, and the stripped particles did not adhere to glass surfaces as one would expect if the AHNs carried a PVP moiety on their surface.

Several slides with Ag NPs were placed in the vacuum chamber for the deposition of different caps via thermal evaporation with one slide being always covered with a mask so that no caps were formed on the surface of Ag NPs on this slide. This slide was treated in the same way as the slides with caps and the stripped particles from this slide were used as a reference in all measurements, including spectroscopic characterization.

Plasmonic AHNs were synthesized with silicon monoxide and lithium fluoride caps as examples of high and low refractive index materials, respectively (Figure 2.1a & Figure 2.1c). Some particles appear in TEM without the caps because they were adsorbed to the TEM grid in the cap-down orientation. The deposition was carried out in the direction normal to the slide surface therefore the caps covered approximately half of the Ag PN surface. It was expected that the deposition of caps with the refractive index n larger than that of the surrounding medium (water, n = 1.33) will result in a red shift of the plasmon resonance compared to the same particles without the caps. The larger the refractive index the larger, though different, the expected shift is for both the dipolar and quadrupolar component of the resonance.[49] The deposition of 20 nm thick SiO caps led to a 20 nm spectral shift of the dipole and a 17 nm shift of the quadrupole (Figure 2.1b). In previous studies, a 20 nm thick silica shell synthesized by the sol-gel chemical method around 80 nm Ag NPs produced a similar, 25 nm red shift.[58] The refractive index of the bulk amorphous silica is 1.46 but the silica shell around Ag NPs had the effective refractive index smaller because the sol-gel layer was hydrated. From this point of view, the observed shift of the resonance in Ag AHNs appeared to be rather small for a typically high n = 1.95 of silicon monoxide films. Even if considering that the silicon monoxide caps cover only half of the NPs surface as compared to the entire surface covered by the silica shell in [58], the AHNs should experience a volume weighted refractive index of ca. 1.6 that still is substantially larger than that of the hydrated silica shell, so that the observed red shift should be larger as well. Based on these numbers, it was concluded that the effective refractive index of the caps on the plasmonic AHNs was

closer to that of amorphous silica than to dense silicon monoxide films, possibly due to the oxidation of SiO into SiO2 in aqueous environment. Also, it is known that the refractive index of silicon monoxide strongly depends on the deposition conditions.[107]

Unexpectedly, LiF caps caused blue shifts for the dipole (16 nm) and quadrupole (4 nm) components of the plasmon resonance (Figure 2.1d) despite the fact that the refractive index of this material (1.4) is also higher than that of water. This behavior can be explained by the large difference in the electric dipole moments of the two materials. Whereas the dipole moment of silica is zero, the dipole moment of lithium fluoride is large, 6.33 Debye.[108] Conceivably, the vectorially oriented lithium fluoride molecules produce at the surface of Ag NPs a static electric field that interacts with the electron density by 'pushing' the electrons from the surface layer more into the interior of the particles or by 'pulling' the electrons more into the surface layer depending on the orientation of the molecules. Both effects alter the effective electron density that participates in the plasmon oscillation thereby causing red or blue spectral shift of the plasmon resonance. A similar interpretation was suggested by Henglein *et al.* to explain the observed shifts in the frequency of the plasmon resonance of Ag NPs upon adsorption of I- and SH- species.[109]

Titanium and aluminum were deposited onto Ag NPs to exemplify the caps with high refractive index materials (Figures 2.2a and 2.2c). Because the direct thermal evaporation of the oxides is difficult, the pure metals were evaporated first and then oxidized upon exposure to the ambient atmosphere and aqueous environment to form titanium dioxide and aluminum oxide caps. The refractive index of both materials

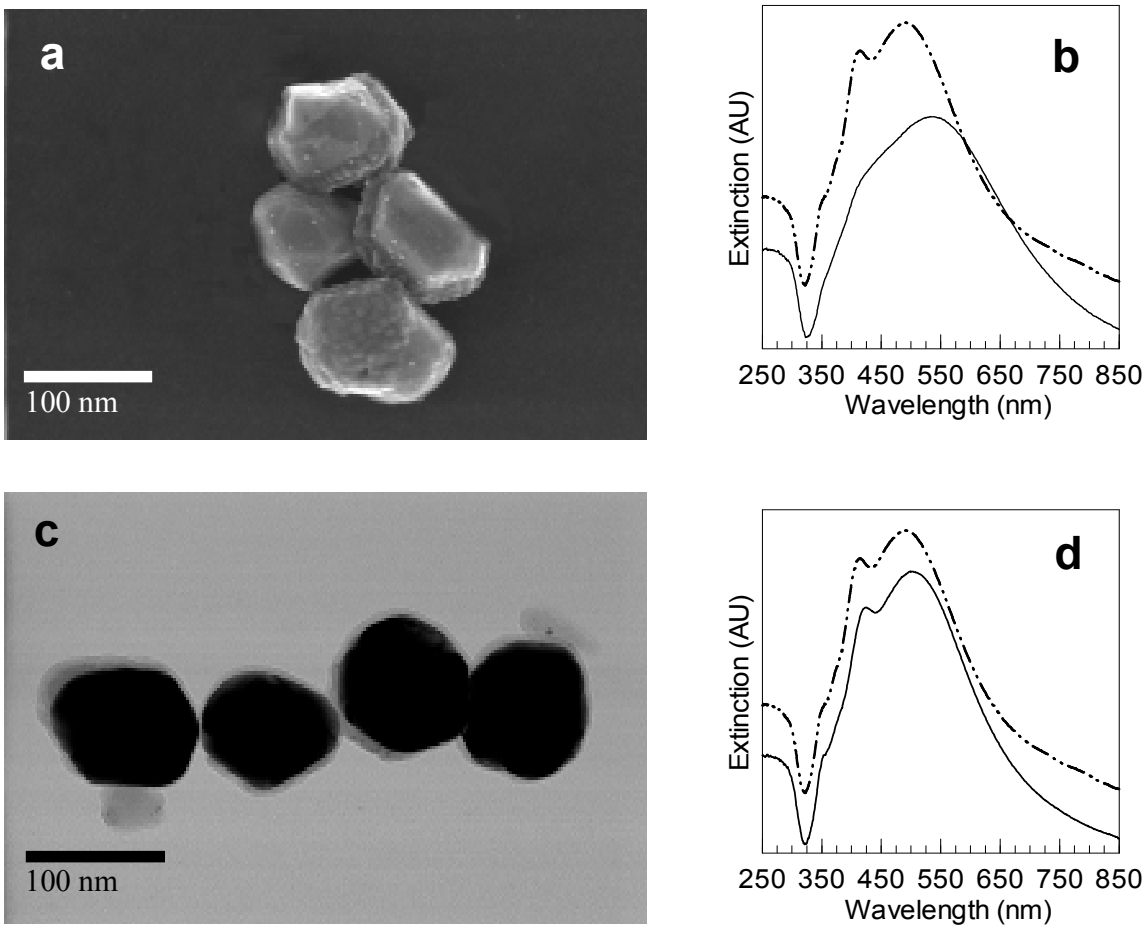

Figure 2.2 TEM and SEM (a, c) and UV-Vis spectra (b, d) of plasmonic AHNs with 10 nm titanium (a, b) and 10 nm aluminum (c, d) caps. Solid curves correspond to plasmonic AHNs and the dashed curves correspond to the same particles without the caps. UV-Vis measurements were performed on stripped particles in water. The spectra in (b, d) are shifted vertically for clarity.

strongly depends on the deposition conditions and is assumed to be around 2 for titania and 1.7 for alumina. A 10 nm cap of titania caused a large, 43 nm red shift of the dipole component of the plasmon resonance (Figure 2.2b) which is commensurate with its high n, whereas the same thickness alumina cap shifted the resonance by only 10 nm. Aluminum is known to form porous oxide layers upon oxidation and the observed small shift was most likely due to this porous hydrated cap.

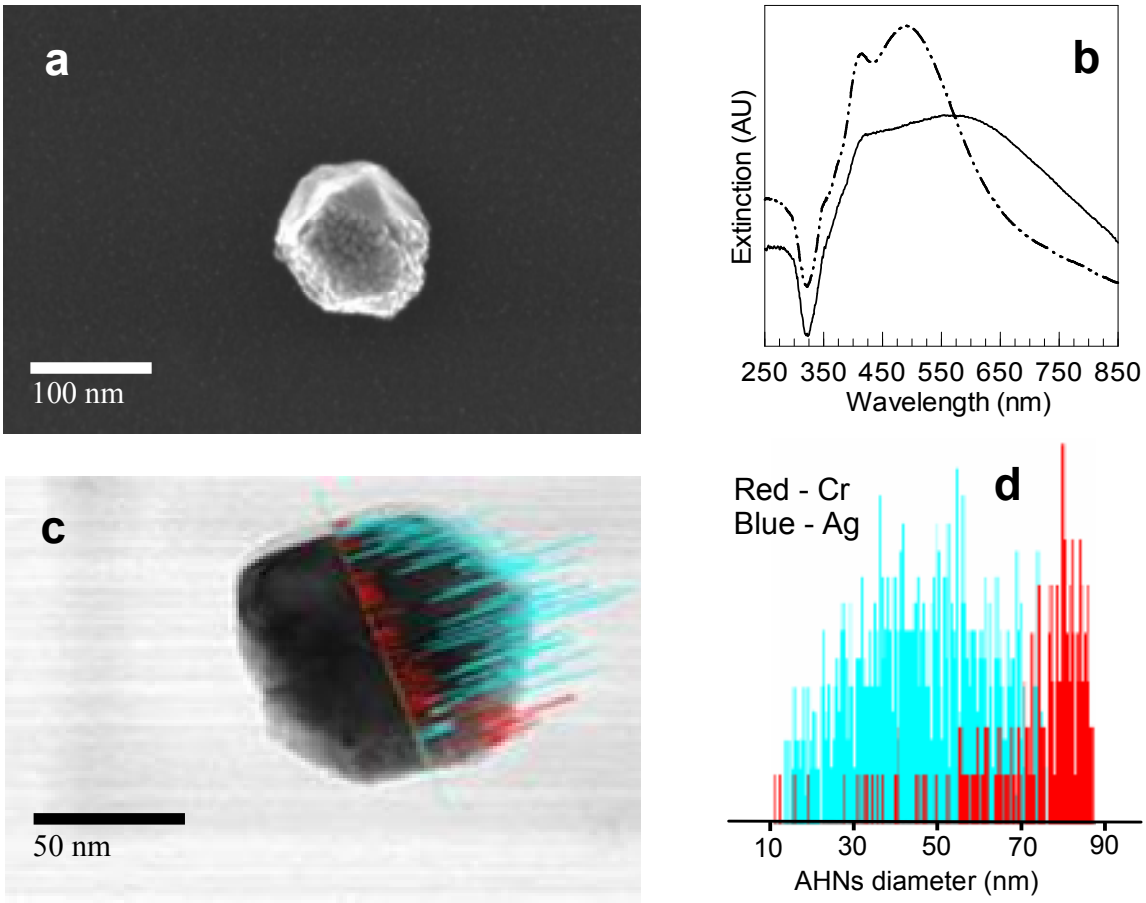

Figure 2.3 SEM (a) and TEM (c), UV-Vis spectra (b), and EDX linescan of plasmonic AHNs with 10 nm chromium caps. The solid line in (b) corresponds to plasmonic AHNs and the dashed line corresponds to the same particles without caps. UV-Vis measurements were performed on stripped particles in water. The spectra in (b) are shifted vertically for clarity.

The AHN technology provides an opportunity for adding magnetic properties to different nanoparticles. For this purpose plasmonic AHNs were synthesized with caps of chromium, nickel, and iron. A 10 nm Cr cap on Ag NPs however did not produce noticeable magnetic properties as concluded from no response of the AHNs suspension to the magnetic field from a permanent magnet. SEM, TEM revealed a cap on the Ag NPs (Figures 2.3a and 2.3c) and the EDX scan confirmed the presence of chromium species on their surface (Figure 2.3d). The lack of magnetic properties indicates that the Cr

metal was oxidized upon exposure to ambient atmosphere and aqueous environment into oxides, most likely Cr (II) and Cr (III) and not into Cr (IV) that is known to be strongly magnetic. X-ray photoelectron spectroscopy (XPS) measurements could be used to confirm this explanation. As can be seen from the SEM image (Figure 2.3a) the cap consisted of small oxide particles. The EDX scan also indicates that the chromium metal did not alloy with Ag NPs during the synthesis and remained on the surface (Figure 2.3c and Figure 2.3d). The red shift of the plasmon in Figure 2.3b is due to the larger refractive index of chromium oxide species relative to that of water.

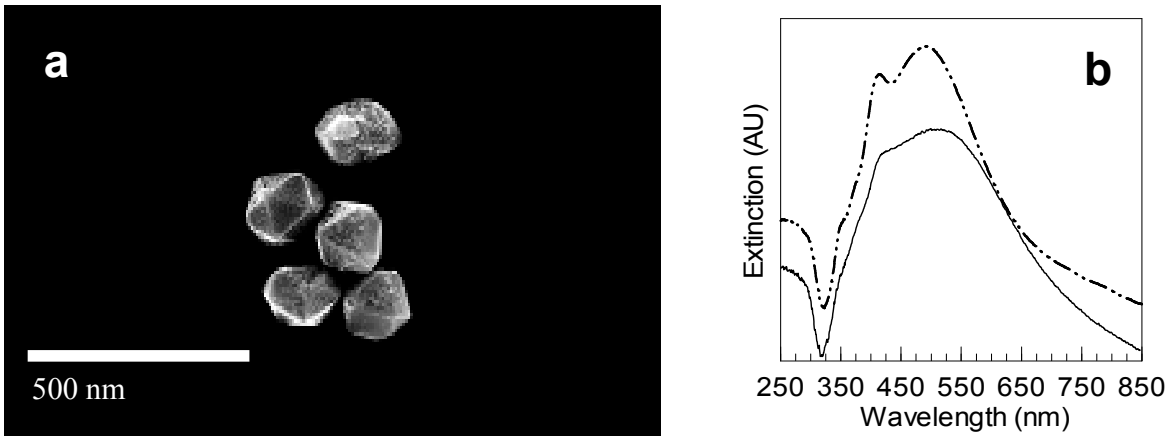

Figure 2.4 SEM (a) and UV-Vis spectra (b) of plasmonic AHNs with 10 nm nickel caps. The solid curve in (b) corresponds to plasmonic AHNs and the dashed curve corresponds to the same particles without caps. UV-Vis measurements were performed on stripped particles in water. The spectra in (b) are shifted vertically for clarity.

The deposition of Ni caps (Figure 2.4) rendered magnetic properties to plasmonic AHNs as was evident from the reversible coagulation of the particles when their aqueous suspension was subjected to a magnetic field gradient. SEM indicated that the cap consisted of small, sub-10 nm particles, most likely of NiO which is known to superparamagnetic.[110, 111] Nickel hydroxide could also exhibit magnetic properties, but is very slightly soluble in water and it is believed that it will dissolve upon transferring

the plasmonic AHNs into an aqueous environment. It can be noted that the deposition of the Ni caps shifted the dipole component of the plasmon resonance by ca. 20 nm (Figure 2.4b) while the chromium caps shifted it by 65 nm. In addition, the plasmon resonance of AHNs with Cr caps is somewhat damped and broadened as compared to Ag NPs without caps (Figure 2.3b). The observed differences between Cr and Ni caps can be explained in terms of the different complex refractive index of the two oxides, specifically their imaginary part (extinction coefficient k). Whereas NiO is a transparent oxide with a low k, chromium oxides are often used as green pigments implying larger k in the visible spectral range. This is only a qualitative argument because it is difficult to speculate on the actual values of n and k of the caps. The refractive index of oxide films is different from that of the bulk materials and strongly depends on the structure of the films and on the deposition conditions used to fabricate the films.

To improve magnetic response of plasmonic AHNs, particles with iron caps were synthesized (Figure 2.5). Direct deposition of 8.3 nm thick Fe caps onto 90 nm Ag NPs made the magnetically induced coagulation of the particles three to four times more efficient than in the case of Ni caps as was determined by the time required for the same volume and the same concentration of plasmonic AHNs to precipitate on the walls of the vessel. However, the particles, while being in non-coagulated state, displayed significant changes in the plasmon, specifically a large red shift and flattening of the dipole component of the resonance as compared to the particles without the caps (Figure 2.5b). Such optical changes could be either due the partial aggregation of the particles in the

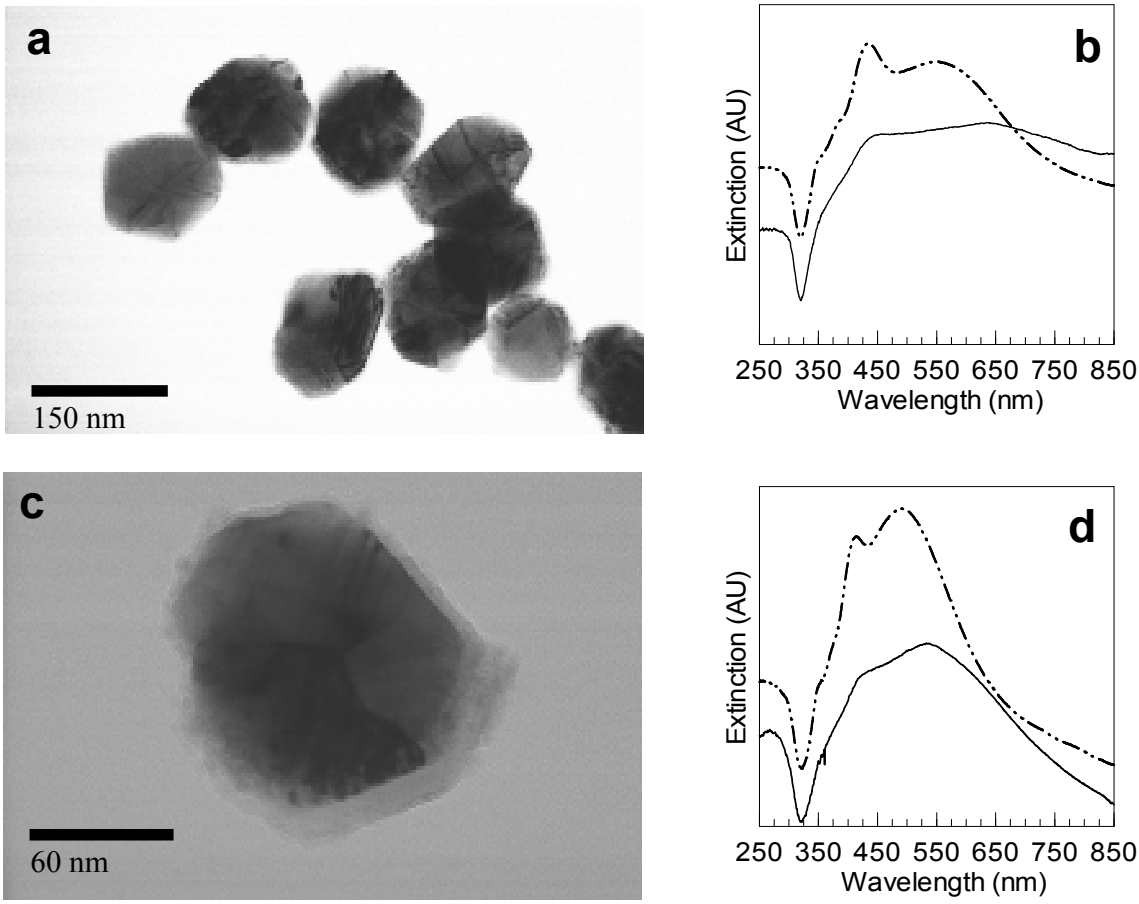

Figure 2.5 TEM (a,c) and UV-Vis spectra (b, d) of plasmonic AHNs with 8.3 nm iron (a, b) and 10 nm iron capped with 10 nm silica (c, d) caps. Solid curves in (b & d) correspond to plasmonic AHNs and the dashed curves correspond to the same particles without the caps. UV-Vis measurements were performed on stripped particles in water. The spectra in (b, d) are shifted vertically for clarity.

suspension or due to the direct effect of the Fe caps on the plasmon resonance of individual particles. Because the magnetically induced particle coagulation was completely reversible resulting in the same spectrum every time (Figure 2.5b, solid line), it was concluded that the observed plasmon changes were caused by the caps. A mixture of superparamagnetic iron oxide species was likely formed after the plasmonic AHNs with Fe caps were dispersed into water. Among different possible oxides, Fe2O3 is a semiconductor with the band gap (2.2 eV) in the visible spectral range.[112] This band gap

introduced additional k to the complex refractive index of the plasmonic AHNs thereby damping the resonance as manifested by a typical spectral behavior seen in Figure 2.5b. In addition to the complex refractive index of the cap, the plasmon resonance is also affected by the direct electronic coupling between conduction electrons in the silver core and the cap. Such coupling is also known to cause red shifts and damping of the plasmon resonance.

To protect iron from oxidation, AHNs were synthesized with Fe caps overcoated with a 10 nm layer of SiO (Figure 2.5c). Even though this approach can potentially render ferromagnetic properties to plasmonic particles, no permanent magnetization was observed in our experiments with a magnet: the magnetically induced coagulation was completely reversible without any additional particle aggregation. Additional aggregation was expected if the residual magnetization in the ferromagnetic caps remained after the removal of the external magnetic field. However, the results of this simple experiment can not be used to completely eliminate the possibility of ferromagnetic properties in these particles. The presence of the 10 nm SiO layer on top of the Fe caps could separate particles sufficiently to prevent their aggregation caused by residual magnetization of the ferromagnetic caps. It was also noted that overcoating the Fe caps with a protective SiO layer reduced the damping of the plasmon resonance (Figure 2.5d) most likely due to the differences in the complex refractive index of Fe metal and its oxides.

The observed plasmon damping by the Fe caps prompted the synthesis of plasmonic

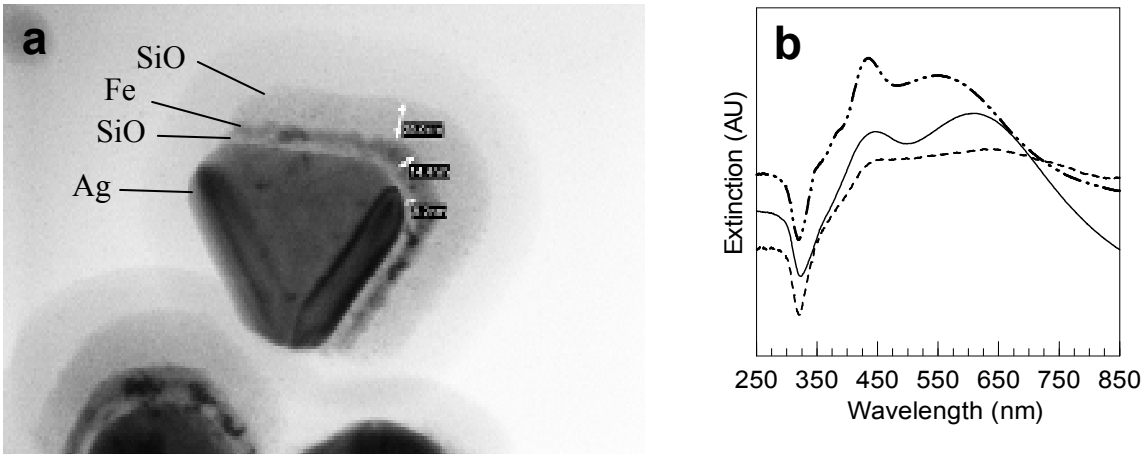

Figure 2.6 TEM (a) and UV-Vis (b) spectra of plasmonic AHNs with 8.2 nm silica caps directly between Ag NPs and a 14.4 nm iron cap which is over-coated with a 25.0 nm silica cap to prevent oxidation. In (b), the solid curve corresponds to plasmonic AHNs and the dashed curve corresponds to the same particles without caps. UV-Vis measurements were performed on stripped particles in water. The spectra in (b) are shifted vertically for clarity. A charging halo is also visible around the particles (a).

AHNs with Fe caps separated from the metal surface by a thin SiO layer (Figure 2.6). As expected, placing a spacing SiO layer between Fe cap and Ag NP surface preserved the resonance in plasmonic AHNs (Figure 2.6b). The effect of the thickness of the spacing layer on the plasmon resonance in AHNs with the Fe cap is shown in Figure 2.7a. The optical measurements were performed on the triple-cap AHNs consisting of a SiO spacer layer of various thicknesses and 10 nm thick Fe cap overcoated with 12 nm thick SiO layer to prevent iron oxidation. The addition of increasingly thicker spacing layers progressively reduced the damping of the resonance, as can be seen from the recovery of the plasmon resonance intensity (Figure 2.7a). At the same time, the resonance continued to shift further into the red spectral range. The largest effects occurred between 0 nm and 2.5 nm thick spacing layers that was attributed to the elimination of the direct electronic coupling between the Fe metal and the Ag core when the 2.5 nm layer was introduced. The increasing red shift was due to the increasing

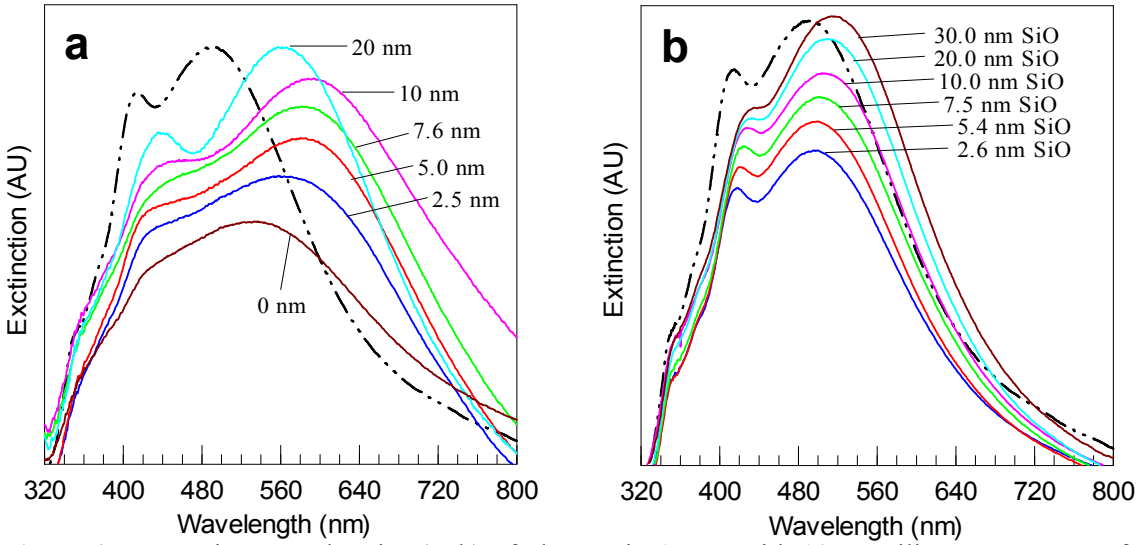

Figure 2.7 UV-Vis spectral series (a, b) of plasmonic AHNs with 10 nm silica caps on top of 10 nm iron caps, and an intermediate layer of silica between the Ag NPs and the iron layer of varying thickness (a) as indicated on each spectra. The same colloid was modified with varying thicknesses of silica caps (b) as indicated for each spectrum. The solid curves correspond to plasmonic AHNs and the dashed curve corresponds to the same particles without caps. Measurements were performed on stripped particles in water.

effective refractive index of the combined of Fe cap and the SiO spacing. However, the rate of this red shift decreased with the increasing thickness of the spacing layer due to the diminishing contribution of the Fe cap to the effective refractive index. At some thickness between 10 and 20 nm, the plasmon started to shift back because the effect of the Fe cap on the plasmon resonance of the silver core was greatly diminished, and the remaining red shift of the AHNs as compared to plasmon resonance position of Ag NPs in water (Figure 2.7a, dashed curve) was caused solely by the thick SiO spacing layer. Note that with the 20 nm spacing layer, the plasmon resonance completely recovered from the damping cause by the Fe cap, and the resultant plasmonic AHNs maintained their strong magnetic properties. The effect of the SiO spacing layer on the resonance of the plasmonic AHNs without the Fe cap is shown in Figure 2.7b for reference.

Finally, plasmonic magnetic AHNs were vectorially oriented on a substrate using a uniform magnetic field. In this experiment, a glass substrate modified with PVP was placed in the contained with the suspension of plasmonic AHNs with Fe caps and the container was further placed into the region of the uniform magnetic field of a permanent magnet. After several hours of the self assembly, the substrate was removed and imaged with SEM revealing the AHNs vectorially oriented on the substrate. Peculiarly, the vast majority of the particles appeared in the cap-down orientation despite the fact the cap-down and cap-up are two equivalent orientations. A possible explanation could be based on slightly different affinity of the Ag core and SiO cap to the PVP modified surface.

Conclusion

It was demonstrated that the AHNs technology enables manipulation of resonance properties of plasmonic nanoparticles. At the same time, new properties can be added as was exemplified by the deposition of the magnetic caps onto the surface of Ag NPs. By placing a dielectric spacer layer between the magnetic cap and the surface of the plasmonic particle the damping of the plasmon resonance by the magnetic material can be avoided. This represents a general strategy for minimizing the interference of the caps with plasmon resonances of the core. Future work related to magnetic plasmonic AHNs will include superconducting quantum interference device (SQUID) and XPS measurements among others for characterizing magnetic properties and the oxidation state of the metals on the surface of the Ag NPs.

CHAPTER THREE

SERS AND RESONANCE ELASTIC SCATTERING FROM CAPPED SINGLE Ag NANOPARTICLES

Introduction

Understanding the mechanism of Surface Enhanced Raman Scattering (SERS) from individual silver nanoparticles (NPs) will provide new insights into the SERS phenomenon, and is essential for the development of novel applications. SERS from single Ag NPs modified with rhodamine 6G was first observed by Nie and Emory[113] and SERS from single Au NPs, nanoshells, and dimers modified with mercaptobenzoic acid was demonstrated by Talley *et al*.[114] Adenine and other biological molecules were also studied on single NPs[115-118], and individual SERS-active NPs were deposited inside living cells to enhance Raman signals from native chemical constituents.[116,119] SERS-active NPs modified with Raman reporter molecules have been utilized as optical labels that provide an attractive alternative to fluorescent labels due to much narrower spectral linewidths as compared to fluorescence emission bands. The narrow Raman linewidths facilitate spectral multiplexing and hyperspectral imaging.[115, 120]

Current understanding of the SERS phenomenon is based on electromagnetic and chemical enhancements mechanisms that, in many cases, act together to produce the overall signal. The electromagnetic enhancement is due to the enhanced local electromagnetic field produced by plasmon resonances excited in metal nanostructures.[86,121-123] The chemical mechanisms are based on specific interactions between molecules and the metal surface leading to an increase of the molecular polarizability.[124] The electromagnetic mechanism can account for up to 10^{11}

enhancement[87], whereas the chemical enhancement is believed to be responsible for only 10^2 – 10^3 contribution to the total SERS signal.[122, 125] Combined, these mechanisms account for the ~10^{14} enhancement observed in single-molecule SERS experiments.[82,85,86,113,118,126-128] Studies of SERS from aggregated metal NPs led to the conclusion that molecules in small gaps between coupled plasmonic structures experience the strongest Raman enhancement. Moskovits and coworkers proposed a theory to explain SERS from aggregated colloids[129] and Kneipp *et al.*[130] demonstrated a correlation between SERS enhancements and different aggregation states of metal NPs. Underlying these observations is the presence of 'hot spots' in the interstitial spaces between the NPs where the local field is particularly concentrated.[59,86,121,130,194] The concept of 'hot spots' was also extended to single plasmonic NPs.[86] The concentrated local field is believed to be responsible for the large (10^{11}) Raman enhancement observed from aggregates and for single molecules immobilized between NP dimers.[66, 131] When chemical enhancement mechanisms are considered, the concept of 'active sites' is used to describe locations on the metal surface where molecular interactions preferentially occur.[113,118,132]

This group has recently introduced another SERS mechanism that unifies plasmon resonances and chemical interactions into a single Raman enhancement cause.[75] Using Ag nanoparticle assemblies on Ag mirror films and a large number of different molecules, plasmon-induced electronic coupling (PIEC) between the molecules and the metal surface was concluded to be the primary source of the Raman enhancement. The advantage of this mechanism is that it accounts for the two main features of SERS: the

dependence upon the chemical nature of the molecules and the requirement to have plasmon resonances. The PIEC model does not exclude other mechanisms such as the local field enhancement and the formation of resonant charge transfer complexes. Here, it is used to explain SERS from capped Ag NPs; however, the PIEC mechanism could have applicability for other SERS systems and may be considered when large Raman enhancements are observed.

Here, a novel SERS-active system referred to as *capped NPs* is described. The capped NPs have a *silver core – molecule – silver cap* structure and present a different type of composite nanoparticles with intriguing optical properties. The PIEC mechanism was invoked as an alternative to the electromagnetic enhancement to explain SERS behavior observed in capped Ag NPs. The SERS-active capped Ag NPs with different Raman reporter molecules can also be used as optical labels; however this aspect is not discussed here.

Experimental

Chemicals: Ag (99.99%) was purchased from Alfa Aesar. 160,000 MW poly(4-vinylpyridine) (PVP), 100,000 - 200,000 MW poly(diallyldimethylammonium chloride (PDDA), 4-aminothiophenol (4-ATP), 4-mercaptobenzoic acid (4-MBA), and adenine were purchased from Aldrich. Reagent alcohol (Ethyl alcohol) was received from Aaper Alcohol and Chemical Company. HF (49%), HNO_3 (70%), and microscope slides and cover slips were obtained from VWR International. Ultra-pure water with 18MΩ·cm resistivity was obtained from a four-bowl Millipore (Milli – Q) water purification system.

Instrumentation: Extinction spectra were measured using a UV-2501PC spectrometer (Shimadzu). SERS measurements and imaging were performed using an Olympus IX71 inverted microscope with a 100x oil immersion objective and type FF immersion oil (Cargille Laboratories, Inc.) coupled to a TRIAX 552 spectrometer equipped with a Symphony, liquid N_2 cooled, spectroscopic grade CCD detector (Horiba-Jobin Yvon) and a thermoelectrically cooled imaging SPOT RT-KE CCD camera (Diagnostic Instruments). A Kr^+ laser (Innova 100, Coherent) was used to excite SERS spectra with 647.1 nm light. Laser intensity at the sample was measured with an 818SL power detector and 1825-C power meter (Newport Corporation). A PR-550 broadband polarization rotator (Newport Corporation) was used to rotate the polarization of the incident laser source. All spectra were processed and figures prepared with Spectra-Solve for Windows software (LasTek Pty. Ltd.).

Synthesis of Ag NPs: Silver nanoparticles (Ag NPs) were synthesized from silver oxide using hydrogen reduction method as described in Reference [105], filtered four times, and stored in deionized water. This method provides full control over the nanoparticle size and surface chemistry because of the lack of any extraneous species associated with the metal surface such as stabilizing agents and/or products of chemical reduction. Nanoparticles can be synthesized with the average dimensions ranging from 30 nm to 300 nm while maintaining good monodispersity, making them a versatile and reliable system for investigating the SERS phenomenon. Ag NPs with the characteristic dimensions 90±5 nm were used in these studies.

Samples: Two types of samples were investigated in this work: *capped NP films* and

single capped NPs. Capped NP films were made by the self-assembly of NPs from aqueous suspensions onto the surface of standard microscope slides modified with PVP or PDDA.[106] Uniform films were formed with a high surface coverage characterized by interparticle distances comparable to the particle size. The films were exposed to 1mM aqueous adenine or ethanoic 4-ATP or 4-MBA solutions (Raman reporters) for 30 minutes followed by thorough rinsing and drying in a stream of N_2 gas. The high concentration of reporter molecules was used to ensure saturation of the metal surface with molecules in a short time period. Care was exercised to prevent particle aggregation caused by capillary forces associated with solvent evaporation. After drying, the films were coated via thermal evaporation with a 10 nm or 20 nm Ag layer in one deposition at normal incidence or by two 10 nm layers in two sequential depositions at $\pm 45^{o}$ angles. The latter procedure is referred to as double angle deposition (DAD). Coating the films with silver resulted in hemispherical caps on the NPs and an interstitial silver layer in the spaces between the particles. The caps were deposited onto the NP surface modified with Raman reporters, thereby resulting in a *silver core – molecule – silver cap* structure. These films were termed *capped NP films* and were investigated for SERS activity or further processed to produce single capped NPs.

Synthesis of Single Capped NPs: NP films capped with 20 nm silver were additionally coated with two 6 nm SiO DAD layers to protect the caps. The NPs with silver and SiO caps were stripped from the slides into solution via mild sonication. The deposited layers were much thinner than the particle diameter and did not bridge to the silver layer between the particles therefore allowing a facile stripping of NPs from the

slides. Next, capped NPs were dried from a low concentration solution onto a clean microscope slide to form a low surface coverage film for single NP SERS investigations. The low surface coverage enabled Raman measurements to be performed with only a single NP within the probe volume. All samples were measured under a glass coverslip with distilled DI water in between.

Raman Measurements: Laser power was 12 μW at the sample focused to ca. 1 μm^2 spot, providing 1.2 kW/cm^2 power density. All reported SERS spectra were recorded with 1 second accumulation time. These parameters were used for NP films, single NPs, and reference samples described below. *Reference samples* were prepared by drying unmodified Ag NPs from a low concentration solution onto the surface of clean slides. After drying, 1 mM aqueous solutions of the Raman reporters were placed on the slides and covered with coverslips. The reference samples were analyzed for Raman scattering at least 30 min after the addition of the Raman reporters to ensure the saturation of the metal surface with the molecules.

Results and Discussion

SERS: Plasmon-induced electronic coupling (PIEC) is a SERS mechanism that combines features of both the electromagnetic and chemical enhancements in that it requires strong interaction of molecules with the metal surface and the excitation of plasmon resonances.[27] One of the goals for the development of SERS-active capped Ag NPs was to obtain more evidence for the PIEC mechanism. Capped NPs were composed of a silver core and a silver cap separated by a monolayer of Raman reporter molecules

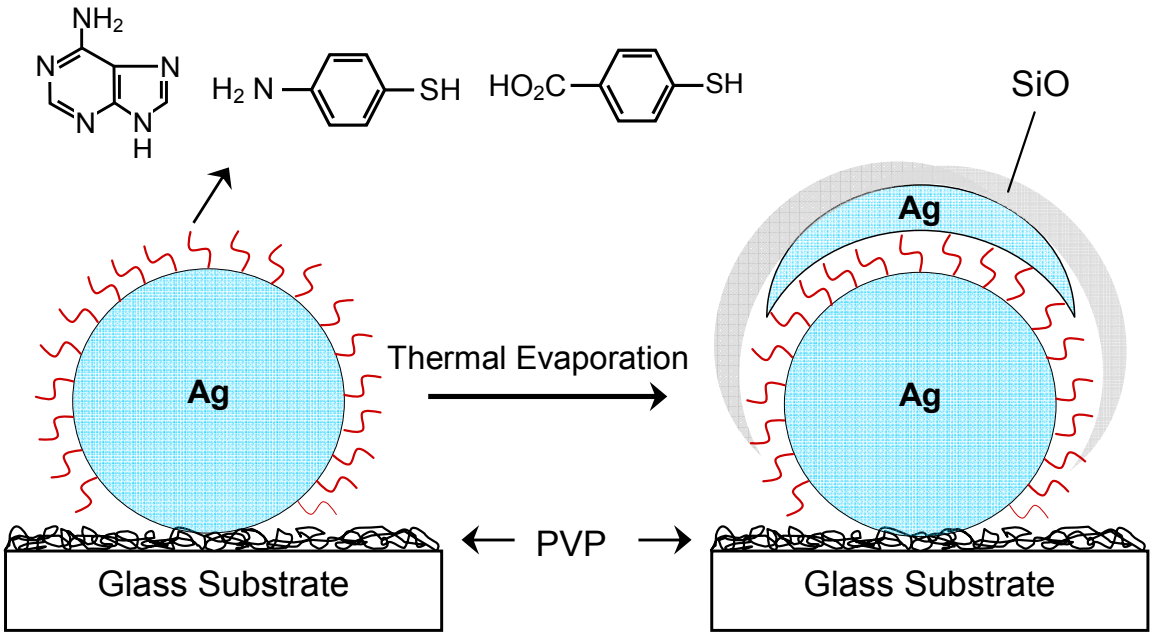

Figure 3.1. A schematic of capped Ag NPs with reporter molecules.

(Figure 3.1). It was expected that the molecules would experience little or no electromagnetic field because the gap between the core and the cap was sufficiently small (0.5 nm) so that strong electronic coupling between the two metal regions should exist. We argue that at distances less than 2 nm between plasmonic structures, direct electronic coupling decreases the local electromagnetic field, despite theoretical predictions to the contrary of a continuously increasing local field strength with decreasing distance.[45,59] In the case of capped NPs, the molecules can be considered as being inside of a conducting medium where the electromagnetic field is largely reduced. As the plasmon resonance is excited in these structures, electrons tunnel through the reporter molecules resulting in strong polarization and the enhancement of the Raman scattering.

Adenine, 4-ATP, and 4-MBA were chosen as the Raman reporters because they exhibit strong affinity to Ag and yield intense and stable SERS signals with characteristic

spectral signatures. It should be noted that adenine and 4-ATP have multiple functionalities such as amines, nitrogens in the purine ring, and the thiol group capable of bridging the core and the cap, whereas 4-MBA has only a single thiol group that anchors the molecule to the core. SERS measurements were obtained from single and DAD capped NP films and compared to those from the uncapped NP films modified with the same reporter molecules. 4-ATP yielded comparable SERS intensities from capped and uncapped films with a slight signal decrease observed for DAD films (Figure 3.2A). SERS of 4-MBA showed a steady signal increase from uncapped to single and then to DAD capped films (Figure 3.2C), whereas SERS from adenine modified films showed a somewhat opposite trend with the strongest signals from the uncapped films (Figure 3.2E). This behavior of the SERS intensity for different reporters in capped films was assumed to be due to the chemical nature of the molecules.

Extinction spectra were also measured in order to explore a possible correlation between the SERS intensity and the excitation of plasmon resonances in the films. The spectra revealed similar behavior for all three reporter molecules: the sharp plasmon peak originated from plasmon coupling[133] slightly decreased upon adsorption of the molecules followed by a much larger decrease after capping. The initial decrease was attributed to the adsorption of the molecules on the surface of the NPs that, most likely, caused changes of the interparticle distance on the films. We have previously shown that plasmon coupling is sensitive to the interparticle distance.[106] It is unlikely that this

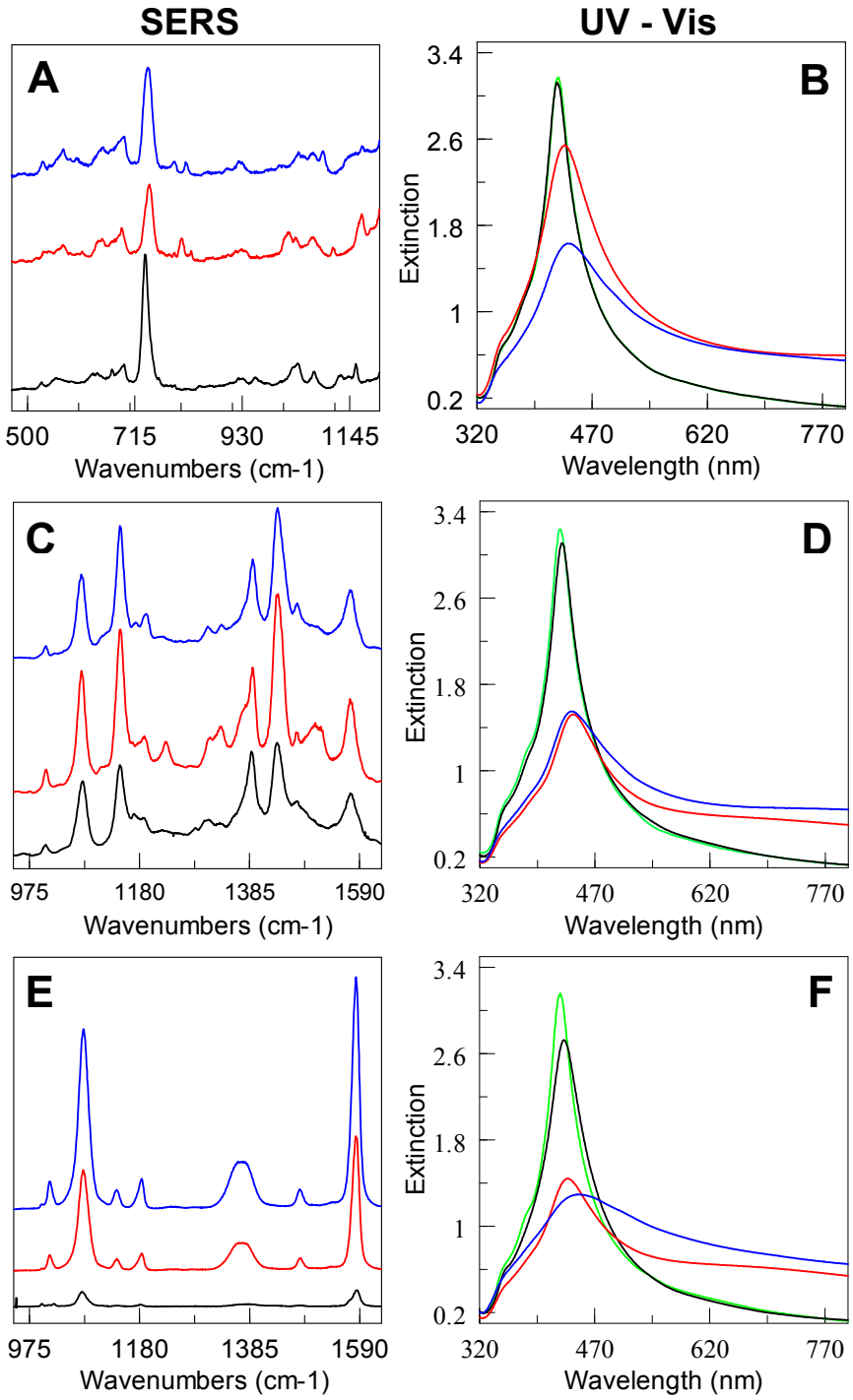

Figure 3.2 SERS spectra (left column) and UV-Vis extinction spectra (right column) of NP films modified with adenine (A,B), 4-ATP (C,D), and 4-MBA (E,F). Individual spectra are labeled as uncapped and unmodified (green), uncapped, modified (black), 10nm Ag single capped (red), and 10nm Ag DAD capped (blue).

initial decrease resulted from increasing the local dielectric function upon adsorption of molecules because it was expected that, in this case, the sharp plasmon peak would increase and red shift. The large decrease of the plasmon peak after capping was attributed to the damping of plasmon coupling by the interstitial Ag layer between the NPs. A noticeable increase of the baseline in the red spectral region was due to the absorption of the interstitial Ag layer. This was verified by measuring extinction spectra of the remaining Ag film after stripping the capped NPs. These spectra were characteristic of thin continuous Ag films (spectra are not shown). The comparison of the SERS intensity with the corresponding extinction spectra and, consequently, with the excitation of plasmon resonances in the films revealed no apparent correlation, thereby suggesting a SERS mechanism different from the local field enhancement.

SERS from the capped films was originated from the NPs and not from the interstitial Ag layer as was concluded from the lack of the measurable SERS signal from the slides after stripping the capped NPs. The effect of the interstitial silver layer on SERS, however, could not be completely ruled out. The SERS signal from the films was also an average from ca. 10 particles present in the excitation volume. For these reasons, SERS was investigated from individual capped NPs to further elucidate the contribution of the caps to the enhancement of Raman scattering.

Single capped NPs were dried onto clean glass slides from a low concentration solution, as described in 'Experimental Section'. Individual particles observed in the microscope were easily discriminated from dimers, oligomers and particle aggregates (Figure 3.3). SERS was only measured from NPs that undoubtedly appeared as single

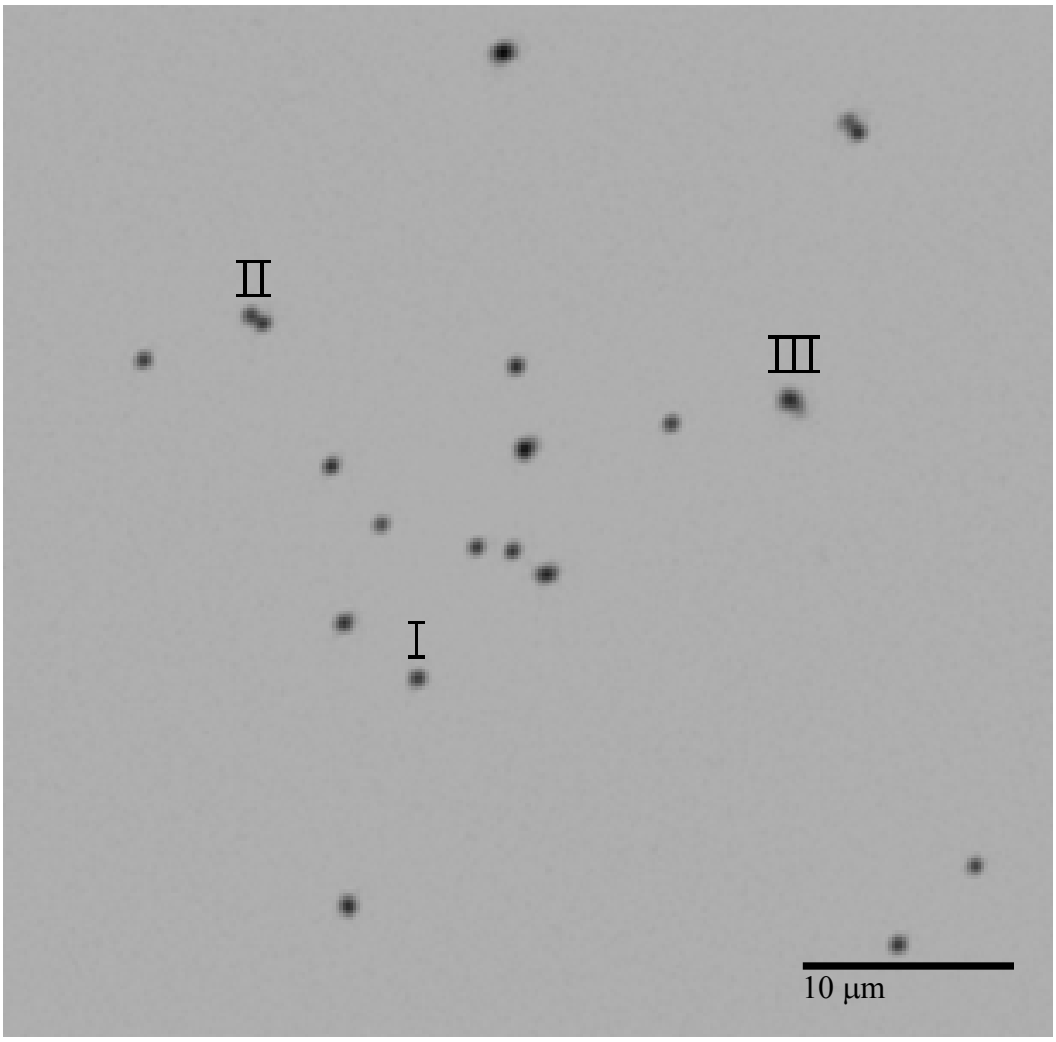

Figure 3.3 A typical microscopy image of individual capped Ag NPs.

particles (I in Figure 3.3) whereas dimers (II in Figure 3.3), aggregates, and other ambiguous structures (III in Figure 3.3) were disregarded.

Single capped NPs produced strong SERS signals for all three reporter molecules when compared to the uncapped reference NPs. It is important to note that the reference NPs were measured in high (1 mM) concentration solutions of the reporters to ensure that the metal surface was fully saturated with molecules. The strongest enhancement due to the addition of the cap was observed for 4-ATP followed by 4-MBA and adenine (Figure

3.4). A very weak SERS signal was measured from 4-ATP when adsorbed on uncapped NPs as compared to capped single NPs (Figure 3.4, middle). On the contrary, the SERS signal from uncapped films modified with 4-ATP was strong and comparable to that from capped films (Figure 3.2C). This fact suggests that the SERS from uncapped films likely originated from sources other than capping, specifically from plasmon coupling between the NPs and from NP clusters formed due to the double functionality of 4-ATP.

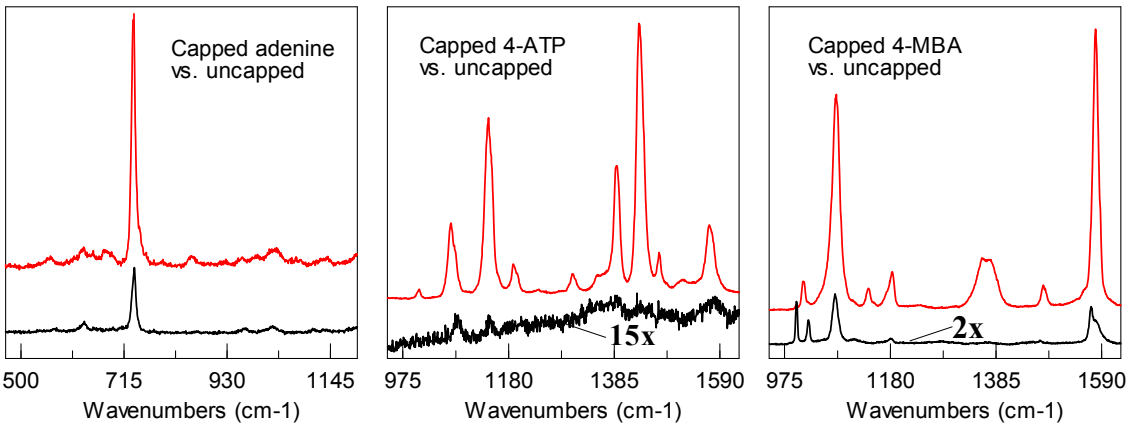

Figure 3.4 Single particle SERS spectra from uncapped (black) and capped (red) NPs. Capped NPs had a single 20 nm Ag cap and a 6 nm SiO DAD cap. Spectra were measured with 1 second accumulation time and 12 μW of 647.1 nm excitation at the sample.

The extinction spectra of single capped NPs modified with reporter molecules were compared to those of single uncapped NPs without reporter molecules (Figure 3.5). Note, that the differences between black (uncapped NPs without reporters) and red (capped NPs with reporters) curves reflect the effect of both surface modification and capping of the NPs. The modification and capping led to an increase of the plasmon extinction at the excitation wavelength (647.1 nm) by 25% for adenine, 34% for 4-ATP, and 38% for 4-MBA. This marginal increase was not commensurate with ca. 5 times increase of the Raman enhancement upon capping for adenine, ca. 8 times for 4-MBA,

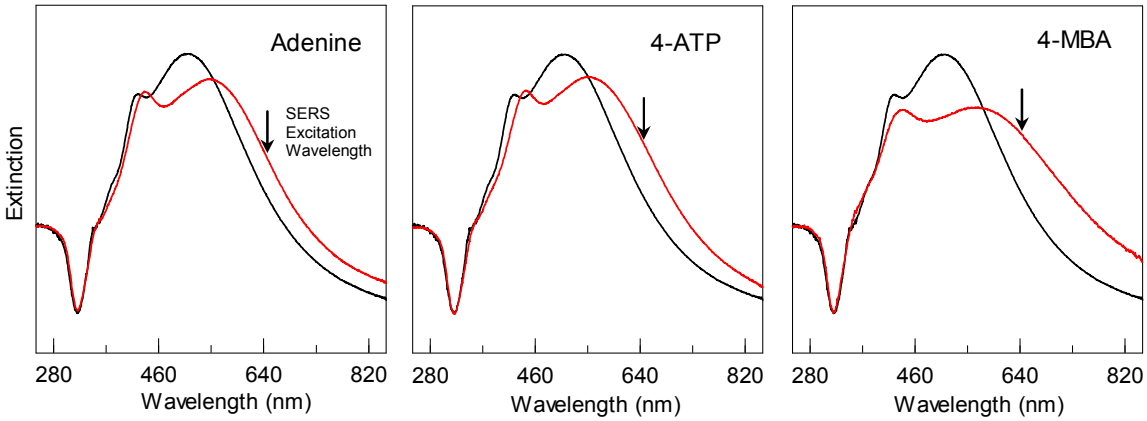

Figure 3.5 Extinction spectra of unmodified uncapped (black) and capped NPs (red) in water. Capped NPs were modified with Raman reporter molecules and capped with 20 nm Ag cap and a 6 nm SiO DAD cap.

and ca. 120 times for 4-ATP. As in the case of the capped NP films, these data indicate that the Raman enhancement should originate from a mechanism other than the local field enhancement.

Plasmon-induced electronic coupling was concluded to be a primary SERS mechanism in capped NPs. Based on this mechanism, chemical bonds between the adsorbed molecules and the metal surface provide a conduction pathway for the oscillating electrons of the plasmon resonance to penetrate into the electronic system of adsorbed molecules. As the oscillating electrons penetrate, they induce strong polarization of the molecules and become 'modulated' with the frequencies of the molecular vibrations. If the plasmon resonance has a scattering component, light will be subsequently scattered with these frequencies. It is important to emphasize that, in this mechanism, the primary source of molecular polarization is the direct electronic coupling with oscillating electrons of the plasmon resonance and not the local and/or incident electromagnetic fields. The Raman scattering is enhanced because the molecular

polarization via direct electron/electron coupling is a more efficient process than the polarization via electron/photon coupling. Plasmon-induced electronic coupling is an exchange type of interaction between free electrons in the metal and the electronic system of the molecules; this interaction is different from a charge transfer, in which the electron is resonantly excited into/from the molecule.[134]

The observed differences in SERS enhancement from different reporter molecules in capped NPs are attributed to the different interactions between the molecules and the metal surface. The strongest enhancement produced by 4-ATP was because this molecule contains two chemical groups capable of strongly interacting with Ag and electronically bridging the core and the cap thereby providing the path of the least resistance for the oscillating electrons. 4-MBA has only one thiol group that strongly interacts with the metal, whereas adenine has even weaker interaction with silver. It was inferred that SERS intensities from single capped Ag NPs reflect the degree to which the oscillating electrons couple to the electronic system of adsorbed molecules.

The SERS enhancement factors were estimated to be ca. 10^8 for adenine molecules in the capped Ag NPs and ca. 10^7 for the molecules adsorbed on uncapped NPs. The calculations assumed 10% collection and detection efficiency for the instrumentation and the optical cross section of a single Ag NP to be 5 times the geometric cross section.[135] The normal Raman scattering cross section of adenine (10^{-30} cm^2/molecule) was taken from Reference [85]. The absolute intensities of the SERS signals scaled as 3×10^3 cps for adenine, 1.7×10^4 cps for 4-ATP, and 2.4×10^4 cps for 4-MBA, respectively under the same experimental conditions and 12 μW laser excitation.

Resonance Elastic Scattering: Capped Ag NPs exhibited strong anisotropic elastic scattering when excited with 647.1 nm light. Approximately 25% of capped NPs dried on microscope slide yielded strong scattering when excited with polarized light. Four images in Figure 3.6 illustrate the progression of the scattered intensity as the laser spot approached a single capped NP. The scattered intensity increased with the overlap of the laser spot and the NP reaching a maximum value when directly over the NP. The intensity at this point saturated the camera and the difference between the intensity of the scattered light from the NP and the scattered intensity from the clean area of the slide exceeded the dynamic range (10^3) of the camera. The remaining ca. 75% of the NPs on the slide displayed varied scattering intensities, all the way down to zero for some NPs, as illustrated in Figure 3.7. Whereas the majority of 'dark' NPs could be made brightly scattering by simply rotating the polarization of the incident light by 90°, some NPs remained dark when excited with any polarization within the plane of the slide. SERS intensity also directly followed the elastic scattering intensity: the stronger the elastic scattering the stronger the SERS. The same scattering behavior was observed for NPs capped with 10 nm and 20 nm caps. In contrast, all uncapped single Ag NPs scattered uniformly at all polarizations (data are not shown).

The observed polarization-dependant light scattering from capped Ag NPs can be rationalized by considering the optical anisotropy induced by the deposition of caps. It is assumed that the addition of a 10 nm thick Ag cap to a 90 nm icosahedral NP does not significantly change its overall shape or the frequency of the dipole plasmon mode along the core-cap axis as compared to the perpendicular dipole mode (Figure 3.5). Otherwise,

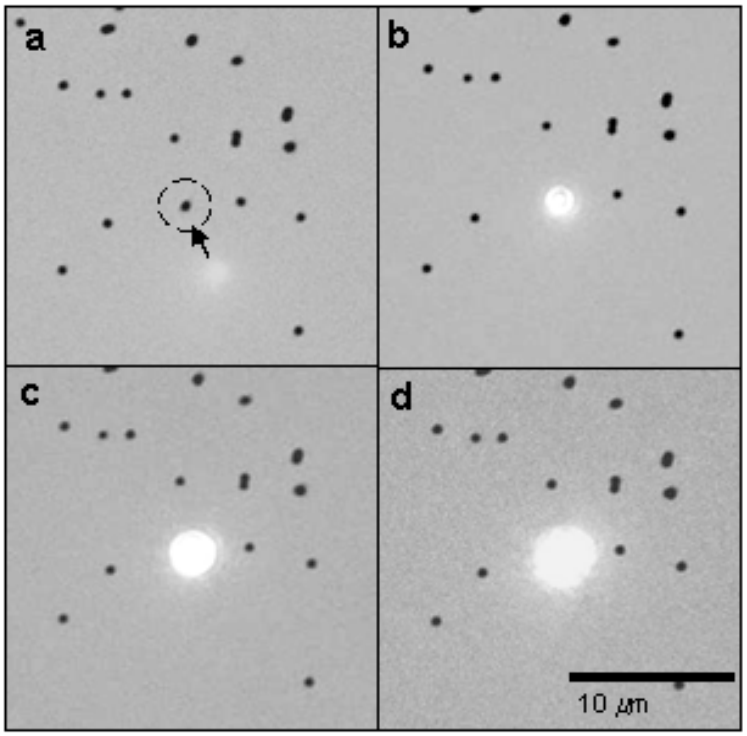

Figure 3.6 Microscopy images of capped NPs as the laser spot approached a 'bright' NP that is indicated with a circle and arrow in (a).

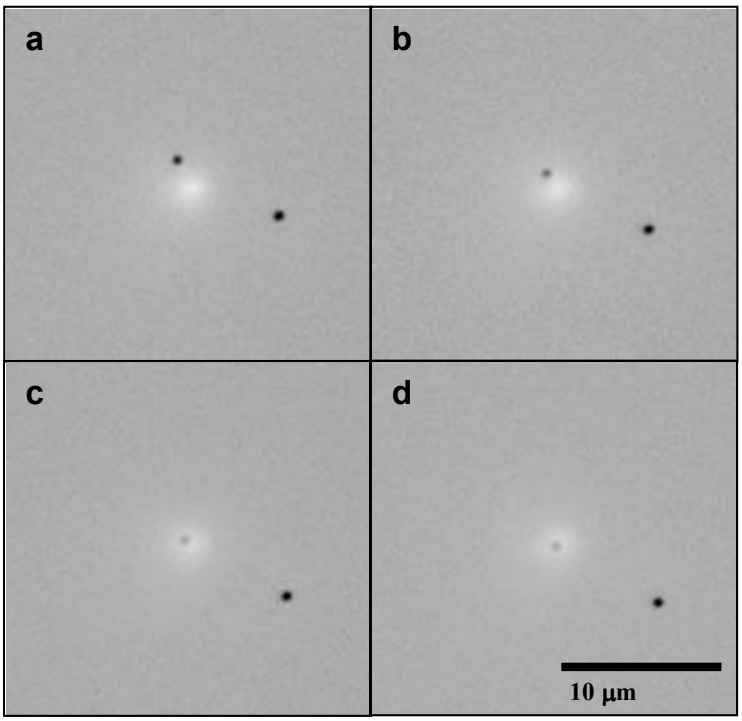

Figure 3.7 Microscopy images of capped NPs as the laser spot approached a 'dark' NP.

as in the case of dimers and elongated NPs, splitting in the extinction spectra would be observed corresponding to longitudinal and transverse modes with different frequencies.[43] The disparities in the scattering along different particle axes could be attributed to the plasmon modes that have similar frequencies but, upon deposition of the cap, have changed their character from radiative to absorbing. There are three degenerate modes corresponding to the electron oscillations along three equal axes in a spherical plasmonic particle. Upon the deposition of the cap, one mode corresponding to the electron oscillations along the core-cap axis becomes different. For capped NPs randomly oriented on glass slides, roughly one third of the particles are expected to be excited along the core-cap axis. If the excitation along this axis results in stronger scattering, one third of the particles would be bright and the two thirds would remain dark. Indeed, ca. 25% of capped Ag NPs were observed to exhibit strong elastic scattering and SERS, thereby suggesting that the NPs were excited along the core-cap axis. This result parallels the increased Raman scattering when excited along the axis connecting two plasmonic NPs in dimers.[59,86,131] We cannot currently speculate why the elastic scattering should be enhanced along this axis and diminished along the other two axes; this will be a subject of future studies.

Conclusions

In conclusion, capped NPs having metal core – molecular layer – metal cap structure present a new type of composite nanoparticles with potentially new properties. In the case of silver metal, capped NPs exhibited strong anisotropic Raman and elastic

scattering when excited with polarized light. Plasmon-induced electronic coupling between the core and the cap was suggested as a main SERS mechanism in this system.

CHAPTER FOUR

Ag NANOPARTICLES AS SCATTERING LABELS FOR FLOW CYTOMETRIC CELL SORTING

Introduction

Cells are the most basic building blocks of all living organisms and a wealth of biological data is stored inside each one. The information available in cells is important to a broad range of bioanalytical studies from cancer research to forensic investigations. A myriad of techniques have been developed to collect information from cells with varying approaches such as homogenization techniques[171,172] or single cell measurements with a microscope.[173,174] Each method has its advantages, however homogenization of tissue samples can average out information about subpopulations, and single cell measurements often lack the high throughput necessary to create a representative model of the tissue as a whole. A more informative approach is to interrogate large numbers of cells individually. To be effective, however, such a method would require high throughput as well as rapid detection and discrimination of cells.

Initially, flow cytometry was developed as a method to rapidly count particles in solution[93] and is now an advanced biochemical tool capable of counting, discriminating, and sorting >10,000 cells per second.[175] In order to discriminate and sort, particles they must be identified via some unique characteristic. Flow cytometry allows particles to be distinguished by several characteristics such as forward and side scattering of light as well as emission from fluorescent-labeled cells.[94, 95] Information about the size and complexity of the cells can be obtained from light scattering measurements, allowing major classes of cells to be discriminated. Fluorescent labels provide the most

information about subpopulations of cells based on the presence of specific receptors that are expressed within the cell or on the cell membrane.

A flow cytometer (FC) is generally composed of three basic systems: fluidics, optics, and electronics. The fluidics system of a FC is responsible for transporting cells, or other particles under investigation into the excitation source and into the area where the separation of cells takes place. Excitation and detection of scattering and fluorescence is accomplished by an optical system whereas electronics are used to for data collection, processing and controlling of components as well as sorting.

In a typical FC experiment, cells are prepared in an electrolyte solution at low concentration to ensure that only a single cell is present in the excitation space at any given time. For stream-in-air methods, the solution containing the cells is hydrodynamically focused into a vibrating stream of droplets by a nozzle tip. As each droplet passes the laser excitation, it scatters or fluoresces. Pre-defined parameters for the scattering and fluorescence are used to discriminate different types of cell by the instrument software. Depending upon the scattering and fluorescence measured from the cells, the electronics can trigger charging plates to electrostatically deflect each droplet into an appropriate container for collection.

The speed of this technique, however, leads to a practical limitation. Because each cell spends only a short time in the excitation space (ca. 10^{-4} sec.), high loading of the fluorescent labels and high excitation power (ca. 200 mW focused into each droplet) are necessary to collect sufficient fluorescence signals. This constraint, in turn, requires that the cells under investigation must have a high number of unique receptors that can be

labeled and used to differentiate them from other cells. Unfortunately, certain receptors are expressed in only a few copies in cells, limiting the number of labels that can be attached per cell. As a result, labeling of these 'rare' receptors may not produce signals strong enough to be used for discrimination, ultimately leading to the requirement of using very bright labels.

Silver nanoparticles (Ag NPs) provide a suitable alternative to fluorescent labels due to their strong interaction with light, specifically their high scattering efficiency. The scattering is so strong that only a single NP is necessary to produce a sufficient signal. This provides an opportunity to label only a small number of receptors and perform efficient sorting. The strength of the scattering from Ag NPs also allows for lower power excitation, therefore inducing less damage to the cells. Here, we introduce a labeling method for cell sorting FC based on the strong light scattering from Ag NPs. An experimental procedure for labeling cells with the NPs is presented and preliminary results are discussed.

Experimental

Chemicals: Ag (99.99%) was purchased from Alfa Aesar. Na_2HPO_4, KH_2PO_4, NaCl, NH_4OH, NaN_3, Tris, Tween 20 (surfactant), 2-propanol, toluene, and DMSO were all purchased from Thermo Fisher Scientific, Incorporated. EtOH was purchased from Pharmco-Aaper and commercial alcohols. Tetraethoxysilane (TEOS) and (3-aminopropyl)tetraethoxysilane (APTES) were purchased from Alfa Aesar and stored under N_2 until used. Hydroxylamine•HCl, E-Z link maleimide activated neutravidin

protein (NAP), *N*-succinimidyl S-acetylthioacetate (SATA), bovine serum albumin (BSA) and biotin were purchased from Pierce, a subsidiary of Thermo Fisher Scientific, Inc. Microscope slides and cover slips were obtained from VWR International. Ultra-pure water with 18MΩ·cm resistivity was obtained from a four-bowl Millipore (Milli – Q) water purification system.

Instrumentation: Extinction spectra were measured using a UV-2501PC spectrometer (Shimadzu). SERS measurements and imaging were performed using an Olympus IX71 inverted microscope with a 100x oil immersion objective and type FF immersion oil (Cargille Laboratories, Inc.) coupled to a thermoelectrically cooled imaging SPOT RT-KE CCD camera (Diagnostic Instruments). A 200 W halogen lamp from SCHOTT AG was used for illumination in scattering mode images.

Sol-gel preparation: A solution of 100 ± 5 nm diameter Ag NPs was prepared in a clean 20 mL glass scintillation vial by diluting 70 μL of concentrated NPs into 15 mL of 2-propanol followed by brief mixing in an ultrasonic bath. The optical density of this solution was measured to be 3.78 a.u. using the UV/visible spectrometer. Next, the solution was degassed by bubbling with N_2 gas for 10 minutes before placing in the ultrasonic bath and adding 2.5 μL of TEOS and 1 mL of Milli-Q H_2O . After degassing the solution with N_2 for another 5 minutes, it was placed in the ultra-sonic bath again where 100 μL of 14.8 M NH_4OH was added dropwise. The vessel was capped and sonicated for an additional 30 seconds and then transferred to a stir plate and stirred for 72 hours to age the silica shells around the NPs. The solution was then centrifuged and washed twice with H_2O and finally centrifuged and re-suspended with 15 mL of fresh 2-

propanol in a clean 20 mL scintillation vial. The optical density of this solution was ca. 2.6 a.u. as measured with the UV/visible spectrometer. After degassing with N_2 for 30 minutes, the vessel was transferred to the ultrasonic bath where 0.5 μL of APTES and 1 mL of H_2O was added to the solution and allowed to mix for 30 seconds under sonication. The solution was degassed again for 5 minutes with N_2 and then transferred back to the ultra-sonic bath where 100 μL of 14.8 M NH_4OH was added dropwise. The vessel was capped and allowed to mix under sonication for 30 seconds before transferring to the stir plate and stirring 16 hours. This solution was centrifuged and re-suspended in H_2O twice for a final optical density of ca. 2.3 a. u..

Neutravidin modification of NPs: A phosphate buffer (PB) was prepared by adding 0.5683 g of Na_2HPO_4 and 0.0980 g of KH_2PO_4 to 0.400 L of Milli-Q H_2O and the pH was adjusted to 7.30 with concentrated H_3PO_4. A 0.1% surfactant solution was prepared by adding 15 μL of Tween to 15 mL of the PB and mixing thoroughly. All vessels used for NP modification were incubated with the Tween solution for 10 minutes and rinsed twice with water prior to use to reduce particle adsorption to the walls of the vessel. 0.5 mg of SATA was measured out and reconstituted in 0.5 mL of DMSO and then transferred to 10mL of PB. 10 μL of this solution was diluted to a volume of 10 mL in PB. Next, 15 μL of this final dilution was added to 0.985 mL of the APTES-modified AgNPs and allowed to incubate in an ultra-sonic bath for 30 minutes. A deacylation solution was prepared by adding 0.348 g of Hydroxylamine•HCL to 8 mL of PB and adjusting the pH to 7.45 with 10 M NaOH. This solution was diluted to a final volume of 10 mL with Milli-Q H_2O. After the SATA incubation with the Ag NPs was complete, the

NP solution was centrifuged and washed 3 times with PB and diluted to a final volume of 1 mL. 100 μL of the deacylation solution was added to the vessel and allowed to react for 2 hours while sonicating. A maleimide conjugation buffer was prepared with 100 mM Na_2HPO_4 and 5 mM EDTA and degassing by mixing under vacuum for 15 minutes prior to use. Next, the NP solution was centrifuged and washed twice with PB and diluted to a final volume of 1.5 mL in PB. 0.5 mg of the E-Z link NAP was reconstituted in 10 mL of the maleimide buffer and 15 μL of this solution was added to the SATA-modified NP solution. This solution was allowed to incubate for 1 hour and then centrifuged and washed with PB twice.

Amine-modified glass slides: Glass microscope slides were cut into 1" x ½" strips, sonicated in EtOH for 10 minutes, rinsed with H_2O, dried at 100 °C for 10 minutes, and plasma cleaned to remove any extraneous organic species from their surface. The slides were then transferred immediately to a 5% APTES solution in toluene for 10 minutes, removed and rinsed with toluene and then acetone, dried with a stream of N_2 and heated at 100 °C for 1 hour immediately prior to use. The presence of amines on the surface was verified by placing a slide into a colloidal solution of unmodified Ag NPs and observing the formation of a monolayer of particles.

Blotting with PA-biotin: A 1 μL spot of maleimide conjugated protective antibody (PA)-biotin was dropped onto the center of glass slide, covered, and allowed to dry. Once dry, blocking buffer was added to the well containing the glass slide. To block a solution of 1 mL of a 50 mM Tris, 150 mM NaCl, 1mg/mL BSA, and .01 % NaN_3 at pH 8 was added and allowed to incubate for 15 minutes at room temperature while mixing.

After blocking, the glass slide was washed 3 times with phosphate buffered saline (PBS) pH 7.3. 1 mL of PBS was left in the well and 100 μL of functionalized Ag-NAP was added to the well. This was allowed to incubate for 30 minutes while mixing. The well was finally washed 10 times with PBS and immediately imaged following the last wash.

Results and Discussion

Silver NPs were synthesized from silver oxide using the hydrogen reduction method as described in Chapter 2 as well as in Reference [105] The hydrogen reduction method can be used to produce NPs with an average diameter ranging from 30 nm to 300 nm while maintaining good monodispersity. In addition, the surface of these Ag NPs is free of organic molecules that could prevent desirable surface modifications. Ag NPs with the characteristic dimensions 100 ± 5 nm were used for this study.

Silica shells were synthesized around the Ag NPs to provide stability, biocompatibility, and a scaffold for surface modification (Figure 4.1). The synthesis was accomplished by hydrolysis and condensation of TEOS resulting in ca. 12 nm in thickness shells. A 1 mL aliquot of these particles was tested in a 200 mM NaCl solution for resistance to particle etching due to the formation of insoluble AgCl. The results showed that after 24 hours of exposure to the salt, the strength of the plasmon band in the extinction spectrum was reduced by only 20%, indicating that the particles were feasible for use as labels in physiological saline concentrations. The final APTES shells were approximately 10 nm in thickness and their presence was verified by adsorption of the modified NPs onto clean Ag films.

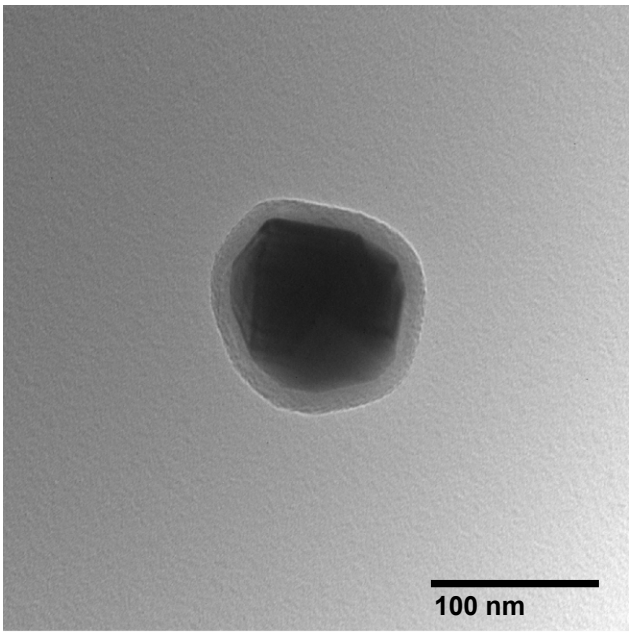

Figure 4.1 Representative ca. 12 nm silica shell around an Ag NP condensed from TEOS.

Modification of the NPs with NAP was carried out in phosphate buffer alone instead of a mixture of phosphate buffer and saline solution to reduce the ionic strength of the solution and minimize particle aggregation. For SATA and NAP modification, a 10:1 molecule:NP stoichiometric ratio was used to ensure sufficient modification of all the particles in solution. Ultra-sonic treatment was also employed to prevent particle aggregation which occurred during the SATA modification and deacylation steps.

Blotting using commercial membranes proved to be inconclusive because of particle entrapment in the roughened surface features that led to high (non-specific binding) backgrounds. For this reason blotting procedures were carried out on glass slides. From Figure 4.2, individual NPs can clearly be seen in darkfield (scattering) mode. Although the particles' physical diameter is less than half of the diffraction limited resolution of the microscope, single particles can be observed due to the fact that they possess a large

scattering cross section that is 10 times larger than their geometric cross section.[37] Brighter spots in the image are small aggregates of particles. These clusters are most likely the result of di-thiol formation of the SATA molecules after deacylation and before the addition of the NAP. When the SATA modification step was performed without ultra-sonication, a highly aggregated suspension resulted.

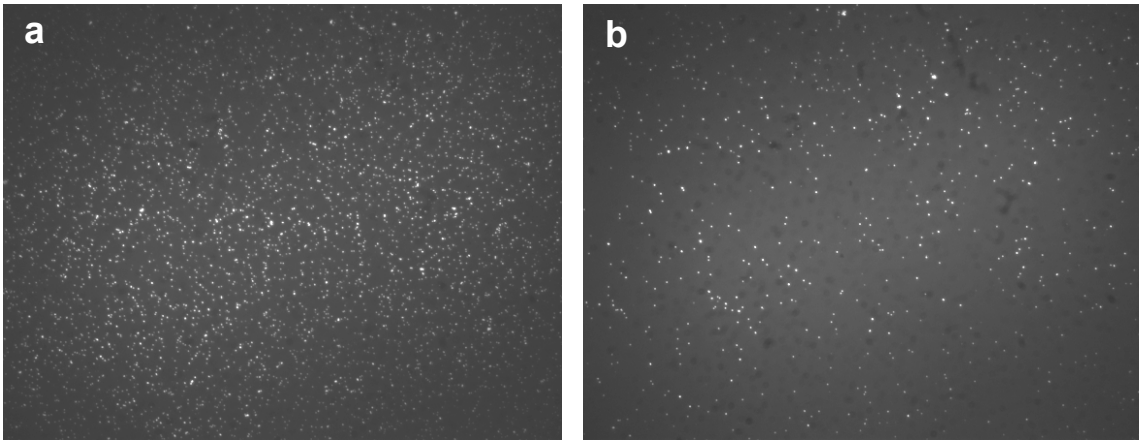

Figure 4.2 Darkfield mode, CCD camera images of NAP-modified Ag NPs. PA-biotin blotted area (a) with a significantly higher density of particles and (b) the unblotted portion of the slide. Slides were blocked with BSA after blotting with a 1 μL aliquot of PA-biotin.

The number of NPs on the blocked, unblotted portion of the slide indicates that either the particles have some non-specific interaction with the BSA, or that the BSA was rinsed away from the amine-modified glass slide during the washing procedures, allowing the NAP-modified NPs to interact directly with the glass surface. The latter explanation is the most probable due to the hydrophobic character of the APTES-modified slide[176], which could have prevented the BSA from forming a tightly packed layer the surface of the slide.

Conclusions

The initial studies presented here illustrate an alternative labeling approach for FC cell sorting. Using Ag NPs as labels capitalizes on their unmatched efficiency for light scattering. The intense scattering signals obtained from these Ag NP labels will enable single-label detection of cells. This advantage allows discrimination of cells based on rare receptors. As such, these labels can potentially replace fluorescent labels for FC methods. An additional bonus is that much lower excitation power can be used, reducing photo-induced damage to the cells. The initial results presented here provide a firm foundation for ongoing research in this area.

CHAPTER 5

CONCLUSIONS AND OUTLOOK

Silver nanostructures possess fundamental properties that make them attractive for a variety of spectroscopic, biological, and technological applications. The work presented in this dissertation focused the synthesis and characterization of nanostructures based on Ag NPs as well as several initial applications. The unique properties of these structures were investigated to assess their potential for optical materials, rationally designed spectroscopic labels, and for a better understanding of the mechanisms responsible for the SERS phenomenon.

The work described in Chapter 2 highlights the development of novel asymmetric hybrid nanoparticles by vacuum deposition of various materials in the form of caps onto Ag NPs. The method developed for the fabrication of asymmetric hybrid NPs provides tunability for the size, shape, and symmetry of the NPs as well as for optical properties and surface chemistry. The ease and reproducibility of this method facilitates fundamental studies of how various caps affect optical properties of the hybrid structures. A number of metal and dielectric caps were deposited on Ag NPs and their effect on the plasmon resonance was systematically investigated. Magnetic properties were rendered in multilayered AHNs containing iron caps. The AHNs provide a unique opportunity for synthesis of multifunctional nanostructures. Though discussed only briefly in the dissertation, AHNs are low symmetry building blocks that can be exploited in the self-assembly of hierarchical architectures. By depositing multiple caps of various materials on the surface of the same NP, different chemical functionalities can be introduced and

further exploited to selectively drive the self-assembly process. Current focus of this project is the deposition of caps made of n- and p-type semiconductor materials and effecting the self-assembly of nanodiodes for photovoltaic applications. The outstanding optical properties of Ag AHNs and wide tunability of their chemical and physical properties make them ideal candidates for many plasmonic technologies.

The proposed and developed new type of optical labels described in Chapter 3 was also based on the AHN platform. These AHNs are composed of an Ag NP core and an Ag cap, separated by a surface-bound layer of Raman-active molecules. These structures were developed with the intent to produce strong SERS from the Raman reporters for bioanalytical applications. It was expected that the contribution from the electromagnetic enhancement mechanism would be minimal because of the mutual proximity of the core and the cap, leading to strong electronic coupling and diminishing of the electromagnetic field between the two. Indeed, a different SERS mechanism, termed the plasmon-induced electronic coupling mechanism, was proposed from these studies and suggested to have general utility to other SERS systems. The generality of this mechanism will have a broad impact on the understanding of the SERS phenomenon and its successful harnessing for further applications. The intense SERS signals observed from these NPs makes them attractive as optical labels in multiplexed bioanalytical assays, which will be the focus of future work. For perspective on this topic, a review of current trends in bioanalytical applications of SERS is presented in Chapter 1.

A different type of Ag NP optical labels is described in Chapter 4. Based on a large cross-section for plasmon excitation, these labels were developed with the goal of

replacing currently used fluorescent labels in flow cytometry. The plasmon resonance of Ag NPs can be tuned to scatter light with efficiencies close to 100% thereby permitting facile optical monitoring of individual NPs. The possibility of using only a single label will allow cells to be differentiated by the presence of 'rare' receptors that are expressed in only a few copies. Current fluorescent labeling techniques require labels to be present in high concentrations to generate sufficient signal for discrimination of cells in high frequency cell sorting applications. An additional advantage is that lower excitation power can be used for detection, rendering less damage to the cells and enabling further analyses to be performed on live cells. Ag NPs were encapsulated in silica shells, modified with amine functionalities, followed by conjugation with neutravidin molecules. Silica shells provided nearly complete protection of Ag core in saline solutions often used in bioanalytical applications. Blotting assays performed with the neutravidin-modified NPs indicated binding of the NPs to the complimentary biotin-labeled area of the glass slides.

Current efforts in this project are focused on optimization of the neutravidin modification with simultaneous reduction of non-specific binding. Future work will include labeling of specific receptors in/on live cells and sorting them with a flow cytometer. If successful, these labels will represent a significant advancement in the field of flow cytometry as well as biological analysis as a whole.

APPENDIX

American Chemical Society's Policy on Theses and Dissertations

If your university requires a signed copy of this letter see contact information below.

Thank you for your request for permission to include **your** paper(s) or portions of text from **your** paper(s) in your thesis. Permission is now automatically granted; please pay special attention to the implications paragraph below. The Copyright Subcommittee of the Joint Board/Council Committees on Publications approved the following:

> Copyright permission for published and submitted material from theses and dissertations
> ACS extends blanket permission to students to include in their theses and dissertations their own articles, or portions thereof, that have been published in ACS journals or submitted to ACS journals for publication, provided that the ACS copyright credit line is noted on the appropriate page(s).
>
> Publishing implications of electronic publication of theses and dissertation material
> Students and their mentors should be aware that posting of theses and dissertation material on the Web prior to submission of material from that thesis or dissertation to an ACS journal may affect publication in that journal. Whether Web posting is considered prior publication may be evaluated on a case-by-case basis by the journal's editor. If an ACS journal editor considers Web posting to be "prior publication", the paper will not be accepted for publication in that journal. If you intend to submit your unpublished paper to ACS for publication, check with the appropriate editor prior to posting your manuscript electronically.

If your paper has **not** yet been published by ACS, we have no objection to your including the text or portions of the text in your thesis/dissertation in **print and microfilm formats**; please note, however, that electronic distribution or Web posting of the unpublished paper as part of your thesis in electronic formats might jeopardize publication of your paper by ACS. Please print the following credit line on the first page of your article: "Reproduced (or 'Reproduced in part') with permission from [JOURNAL NAME], in press (or 'submitted for publication'). Unpublished work copyright [CURRENT YEAR] American Chemical Society." Include appropriate information.

If your paper has already been published by ACS and you want to include the text or portions of the text in your thesis/dissertation in **print or microfilm formats**, please print the ACS copyright credit line on the first page of your article: "Reproduced (or 'Reproduced in part') with permission from [FULL REFERENCE CITATION.] Copyright [YEAR] American Chemical Society." Include appropriate information.

Submission to a Dissertation Distributor: If you plan to submit your thesis to UMI or to another dissertation distributor, you should not include the unpublished ACS paper in your thesis if the thesis will be disseminated electronically, until ACS has published your paper. After publication of the paper by ACS, you may release the entire thesis (**not the individual ACS article by itself**) for electronic dissemination through the distributor; ACS's copyright credit line should be printed on the first page of the ACS paper.

Use on an Intranet: The inclusion of your ACS unpublished or published manuscript is permitted in your thesis in print and microfilm formats. If ACS has published your paper you may include the manuscript in your thesis on an intranet that is not publicly available. Your ACS article cannot be posted electronically on a publicly available medium (i.e. one that is not password protected), such as but not limited to, electronic archives, Internet, library server, etc. The only material from your paper that can be posted on a public electronic medium is the article abstract, figures, and tables, and you may link to the article's DOI or post the article's author-directed URL link provided by ACS. This paragraph does not pertain to the dissertation distributor paragraph above.

Questions? Call +1 202/872-4368/4367. Send e-mail to copyright@acs.org or fax to +1 202-776-8112.

10/10/03, 01/15/04, 06/07/06

REFERENCES

[1] L. Baia, M. Baia, J. Popp, S. Astilean, *Journal of Physical Chemistry B* **2006**, *110*, 23982.

[2] J. A. Dieringer, A. D. McFarland, N. C. Shah, D. A. Stuart, A. V. Whitney, C. R. Yonzon, M. A. Young, X. Y. Zhang, R. P. Van Duyne, *Faraday Discussions* **2006**, *132*, 9.

[3] W. E. Doering, M. E. Piotti, M. J. Natan, R. G. Freeman, *Advanced Materials* **2007**, *19*, 3100.

[4] J. W. Hu, B. Zhao, W. Q. Xu, Y. G. Fan, B. F. Li, Y. Ozaki, *Journal of Physical Chemistry B* **2002**, *106*, 6500.

[5] S. Hudson, G. Chumanov, *The Journal of Physical Chemistry, C* **2008**, *Manuscript accepted for publication*.

[6] J. Kneipp, H. Kneipp, K. Kneipp, *Chemical Society Reviews* **2008**, *37*, 1052.

[7] A. Otto, *Surface Science* **1982**, *117*, 330.

[8] R. A. Tripp, R. A. Dluhy, Y. P. Zhao, *Nano Today* **2008**, *3*, 31.

[9] D. S. Citrin, *Nano Letters* **2005**, *5*, 985.

[10] M. W. Knight, N. K. Grady, R. Bardhan, F. Hao, P. Nordlander, N. J. Halas, *Nano Letters* **2007**, *7*, 2346.

[11] J. R. Krenn, *Nature Materials* **2003**, *2*, 210.

[12] S. A. Maier, P. G. Kik, H. A. Atwater, *Applied Physics Letters* **2002**, *81*, 1714.

[13] I. D. Mayergoyz, Z. Y. Zhang, *Ieee Transactions on Magnetics* **2007**, *43*, 1685.

[14] R. Sainidou, F. J. G. de Abajo, *Optics Express* **2008**, *16*, 4499.

[15] J. J. Xiao, K. Yakubo, K. W. Yu, *Applied Physics Letters* **2006**, *89*.

[16] Z. Xinping, L. Hongmei, T. Jinrong, S. Yanrong, W. Li, S. Jiaoyang, Z. Guozhen, *Nanotechnology* **2008**, 285202 (6 pp.).

[17] M. Dragoman, D. Dragoman, *Progress in Quantum Electronics* **2008**, *32*, 1.

[18] S. A. Maier, M. L. Brongersma, P. G. Kik, S. Meltzer, A. A. G. Requicha, H. A. Atwater, *Advanced Materials* **2001**, *13*, 1501.

[19] J. K. Daniels, T. P. Caldwell, K. A. Christensen, G. Chumanov, *Analytical Chemistry* **2006**, *78*, 1724.

[20] D. D. Evanoff, J. Heckel, T. P. Caldwell, K. A. Christensen, G. Chumanov, *Journal of the American Chemical Society* **2006**, *128*, 12618.

[21] J. I. Jerez-Rozo, O. M. Primera-Pedrozo, M. A. Barreto-Caban, S. P. Hernandez-Rivera, *IEEE Sensors Journal* **2008**, 974.

[22] S. Malynych, G. Chumanov, *Journal of Optics a-Pure and Applied Optics* **2006**, *8*, S144.

[23] O. M. Primera-Pedrozo, J. I. Jerez-Rozo, E. De La Cruz-Montoya, T. Luna-Pineda, L. C. Pacheco-Londono, S. P. Hernandez-Rivera, *IEEE Sensors Journal* **2008**, 963.

[24] M. E. Stewart, C. R. Anderton, L. B. Thompson, J. Maria, S. K. Gray, J. A. Rogers, R. G. Nuzzo, *Chemical Reviews* **2008**, *108*, 494.

[25] D. A. Stuart, J. M. Yuen, N. S. O. Lyandres, C. R. Yonzon, M. R. Glucksberg, J. T. Walsh, R. P. Van Duyne, *Analytical Chemistry* **2006**, *78*, 7211.

[26] C. E. Talley, L. Jusinski, C. W. Hollars, S. M. Lane, T. Huser, *Analytical Chemistry* **2004**, *76*, 7064.
[27] F. Yan, T. Vo-Dinh, *Sensors and Actuators B-Chemical* **2007**, *121*, 61.
[28] X. H. Huang, P. K. Jain, I. H. El-Sayed, M. A. El-Sayed, *Lasers in Medical Science* **2008**, *23*, 217.
[29] L. Au, D. S. Zheng, F. Zhou, Z. Y. Li, X. D. Li, Y. N. Xia, *Acs Nano* **2008**, *2*, 1645.
[30] M. Chen, Y. N. Kim, H. M. Lee, C. Li, S. O. Cho, *Journal of Physical Chemistry C* **2008**, *112*, 8870.
[31] A. M. Schwartzberg, J. Z. Zhang, *Journal of Physical Chemistry C* **2008**, *112*, 10323.
[32] V. Subramanian, E. Wolf, P. V. Kamat, *Journal of Physical Chemistry B* **2001**, *105*, 11439.
[33] S. Pillai, K. R. Catchpole, T. Trupke, M. A. Green, *Journal of Applied Physics* **2007**, *101*.
[34] K. R. Catchpole, S. Pillai, *Journal of Luminescence* **2006**, *121*, 315.
[35] C. Hagglund, M. Zach, B. Kasemo, *Applied Physics Letters* **2008**, *92*.
[36] B. V. K. Naidu, J. S. Park, S. C. Kim, S. M. Park, E. J. Lee, K. J. Yoon, S. J. Lee, J. W. Lee, Y. S. Gal, S. H. Jin, *Solar Energy Materials and Solar Cells* **2008**, *92*, 397.
[37] D. D. Evanoff, G. Chumanov, *Journal of Physical Chemistry B* **2004**, *108*, 13957.
[38] O. Muskens, D. Christofilos, N. Del Fatti, F. Vallee, *Journal of Optics a-Pure and Applied Optics* **2006**, *8*, S264.
[39] U. Kreibig, M. Vollmer, *Optical Properties of Metal Clusters, Vol. 25*, Springer, Berlin, **1995**.
[40] D. D. Evanoff, G. Chumanov, *Chemphyschem* **2005**, *6*, 1221.
[41] S. A. Maier, H. A. Atwater, *Journal of Applied Physics* **2005**, *98*.
[42] K. Hering, D. Cialla, K. Ackermann, T. Dorfer, R. Moller, H. Schneidewind, R. Mattheis, W. Fritzsche, P. Rosch, J. Popp, *Analytical and Bioanalytical Chemistry* **2008**, *390*, 113.
[43] T. A. El-Brolossy, T. Abdallah, M. B. Mohamed, S. Abdallah, K. Easawi, S. Negm, H. Talaat, *European Physical Journal-Special Topics* **2008**, *153*, 361.
[44] X. G. Hu, T. Wang, L. Wang, S. J. Dong, *Journal of Physical Chemistry C* **2007**, *111*, 6962.
[45] K. L. Kelly, E. Coronado, L. L. Zhao, G. C. Schatz, *Journal of Physical Chemistry B* **2003**, *107*, 668.
[46] S. Link, M. A. El-Sayed, *Journal of Physical Chemistry B* **1999**, *103*, 8410.
[47] A. Sabur, M. Havel, Y. Gogotsi, *Journal of Raman Spectroscopy* **2008**, *39*, 61.
[48] G. Mie, *Annalen der Physik IV* **1908**, *25*, 377.
[49] A. S. Kumbhar, M. K. Kinnan, G. Chumanov, *Journal of the American Chemical Society* **2005**, *127*, 12444.
[50] A. J. Haes, J. Zhao, S. L. Zou, C. S. Own, L. D. Marks, G. C. Schatz, R. P. Van Duyne, *Journal of Physical Chemistry B* **2005**, *109*, 11158.

[51] A. M. Schwartzberg, T. Y. Oshiro, J. Z. Zhang, T. Huser, C. E. Talley, *Analytical Chemistry* **2006**, *78*, 4732.
[52] J. C. Love, B. D. Gates, D. B. Wolfe, K. E. Paul, G. M. Whitesides, *Nano Letters* **2002**, *2*, 891.
[53] L. Zhou, X. F. Yu, X. F. Fu, Z. H. Hao, K. Y. Li, *Chinese Physics Letters* **2008**, *25*, 1776.
[54] X. H. Huang, I. H. El-Sayed, W. Qian, M. A. El-Sayed, *Nano Letters* **2007**, *7*, 1591.
[55] S. Link, M. B. Mohamed, M. A. El-Sayed, *Journal of Physical Chemistry B* **1999**, *103*, 3073.
[56] W. Ni, X. Kou, Z. Yang, J. F. Wang, *Acs Nano* **2008**, *2*, 677.
[57] L. Yu, G. L. Liu, K. Jaeyoun, Y. X. Mejia, L. P. Lee, *Nano Letters|Nano Letters* **2005**, *5*, 119.
[58] D. D. Evanoff, R. L. White, G. Chumanov, *Journal of Physical Chemistry B* **2004**, *108*, 1522.
[59] E. Hao, G. C. Schatz, *Journal of Chemical Physics* **2004**, *120*, 357.
[60] I. Abdulhalim, M. Zourob, A. Lakhtakia, *Electromagnetics* **2008**, *28*.
[61] S. Basu, S. Jana, S. Pande, T. Pal, *Journal of Colloid and Interface Science* **2008**, *321*, 288.
[62] S. Link, Z. L. Wang, M. A. El-Sayed, *Journal of Physical Chemistry B* **1999**, *103*, 3529.
[63] G. V. P. Kumar, S. Shruthi, B. Vibha, B. A. A. Reddy, T. K. Kundu, C. Narayana, *Journal of Physical Chemistry C* **2007**, *111*, 4388.
[64] Y. Liang, J. L. Gong, Y. Huang, Y. Zheng, J. H. Jiang, G. L. Shen, R. Q. Yu, *Talanta* **2007**, *72*, 443.
[65] I. I. S. Lim, P. N. Njoki, H. Y. Park, X. Wang, L. Y. Wang, D. Mott, C. J. Zhong, *Nanotechnology* **2008**, *19*.
[66] L. Sun, K. B. Sung, C. Dentinger, B. Lutz, L. Nguyen, J. W. Zhang, H. Y. Qin, M. Yamakawa, M. Q. Cao, Y. Lu, A. J. Chmura, J. Zhu, X. Su, A. A. Berlin, S. Chan, B. Knudsen, *Nano Letters* **2007**, *7*, 351.
[67] J. N. Anker, W. P. Hall, O. Lyandres, N. C. Shah, J. Zhao, R. P. Van Duyne, *Nature Materials* **2008**, *7*, 442.
[68] J. D. Driskell, S. Shanmukh, L. Yong-Jun, S. Hennigan, L. Jones, Z. Yi-Ping, R. A. Dluhy, D. C. Krause, R. A. Tripp, *IEEE Sensors Journal* **2008**, 863.
[69] C. Girard, *Reports on Progress in Physics* **2005**, *68*, 1883.
[70] J. R. Krenn, B. Lamprecht, H. Ditlbacher, G. Schider, M. Salerno, A. Leitner, F. R. Aussenegg, *Europhysics Letters* **2002**, *60*, 663.
[71] H. A. Atwater, S. Maier, A. Polman, J. A. Dionne, L. Sweatlock, *Mrs Bulletin* **2005**, *30*, 385.
[72] S. A. Maier, *Ieee Journal of Selected Topics in Quantum Electronics* **2006**, *12*, 1671.
[73] J. K. Daniels, G. Chumanov, *Journal of Physical Chemistry B* **2005**, *109*, 17936.
[74] G. Chumanov, K. Sokolov, T. M. Cotton, *Journal of Physical Chemistry* **1996**, *100*, 5166.

[75] M. K. Kinnan, G. Chumanov, *Journal of Physical Chemistry C* **2007**, *111*, 18010.
[76] J. A. Stroscio, D. M. Eigler, *Science* **1991**, *254*, 1319.
[77] P. Dieska, I. Stich, R. Perez, *Physical Review Letters* **2005**, *95*.
[78] S. Malynych, G. Chumanov, *Journal of Microscopy-Oxford* **2008**, *229*, 567.
[79] H. Nakashima, K. Furukawa, Y. Kashimura, K. Torimitsu, *Langmuir* **2008**, *24*, 5654.
[80] Z. Jia, R. D. K. Misra, *Materials Technology* **2008**, *23*, 66.
[81] M. Sachan, C. Bonnoit, C. Hogg, E. Evarts, J. A. Bain, S. A. Majetich, J. H. Park, J. G. Zhu, *Journal of Physics D: Applied Physics* **2008**, 134001 (5 pp.).
[82] S. R. Emory, R. A. Jensen, T. Wenda, M. Y. Han, S. M. Nie, *Faraday Discussions* **2006**, *132*, 249.
[83] J. Jiang, K. Bosnick, M. Maillard, L. Brus, *Journal of Physical Chemistry B* **2003**, *107*, 9964.
[84] K. Kneipp, Y. Wang, H. Kneipp, L. T. Perelman, I. Itzkan, R. Dasari, M. S. Feld, *Physical Review Letters* **1997**, *78*, 1667.
[85] K. Kneipp, H. Kneipp, V. B. Kartha, R. Manoharan, G. Deinum, I. Itzkan, R. R. Dasari, M. S. Feld, *Physical Review E* **1998**, *57*, R6281.
[86] H. X. Xu, J. Aizpurua, M. Kall, P. Apell, *Physical Review E* **2000**, *62*, 4318.
[87] K. Kneipp, H. Kneipp, J. Kneipp, *Accounts of Chemical Research* **2006**, *39*, 443.
[88] R. J. C. Brown, J. Wang, R. Tantra, R. E. Yardley, M. J. T. Milton, *Faraday Discussions* **2006**, *132*, 201.
[89] P. Kambhampati, C. M. Child, M. C. Foster, A. Campion, *Journal of Chemical Physics* **1998**, *108*, 5013.
[90] Fleischm.M, P. J. Hendra, McQuilla.Aj, *Chemical Physics Letters* **1974**, *26*, 163.
[91] M. G. Albrecht, J. A. Creighton, *Journal of the American Chemical Society* **1977**, *99*, 5215.
[92] D. L. Jeanmaire, R. P. Vanduyne, *Journal of Electroanalytical Chemistry* **1977**, *84*, 1.
[93] P. J. Crosland-Taylor, *Nature* **1953**, *171*, 37.
[94] O. Resina-Pelfort, J. Comas-Riu, J. Vives-Rego, *Systematic and Applied Microbiology* **2001**, *24*, 31.
[95] W. J. Parak, T. Pellegrino, C. Plank, *Nanotechnology* **2005**, *16*, R9.
[96] J. Q. Liu, A. I. Maaroof, L. Wieczorek, M. B. Cortie, *Advanced Materials* **2005**, *17*, 1276.
[97] M. A. Correa-Duarte, V. Salgueirino-Maceira, B. Rodriguez-Gonzalez, L. M. Liz-Marzan, A. Kosiorek, W. Kandulski, M. Giersig, *Advanced Materials* **2005**, *17*, 2014.
[98] R. R. Agayan, T. Horvath, B. H. McNaughton, A. J.N., R. Kopelman, *Proc. SPIE (International Society of Photonic Engineering)* **2004**, *5514*, 502.
[99] M. Himmelhaus, H. Takei, *Physical Chemistry Chemical Physics* **2002**, *4*, 496.
[100] J. N. Anker, R. Kopelman, *Applied Physics Letters* **2003**, *82*, 1102.
[101] H. Zabel, *Journal of Physics-Condensed Matter* **1999**, *11*, 9303.
[102] S. M. Rossnagel, *Journal of Vacuum Science & Technology A* **2003**, *21*, S74.
[103] P. D. Cozzoli, L. Manna, *Nature Materials* **2005**, *4*, 801.

[104] T. Mokari, C. G. Sztrum, A. Salant, E. Rabani, U. Banin, *Nature Materials* **2005**, *4*, 855.
[105] D. D. Evanoff, G. Chumanov, *Journal of Physical Chemistry B* **2004**, *108*, 13948.
[106] S. Malynych, G. Chumanov, *Journal of the American Chemical Society* **2003**, *125*, 2896.
[107] K. W. Wecht, *Applied Optics* **1991**, *30*, 4133.
[108] NIST, in *Computational Chemistry*, March 30, 2007 ed., NIST, **2007**, p. http://srdata.nist.gov/cccbdb/.
[109] T. Linnert, P. Mulvaney, A. Henglein, *Journal of Physical Chemistry* **1993**, *97*, 679.
[110] T. Ahmad, K. V. Ramanujachary, S. E. Lofland, A. K. Ganguli, *Solid State Sciences* **2006**, *8*, 425.
[111] Y. Ichiyanagi, N. Wakabayashi, J. Yamazaki, S. Yamada, Y. Kimishima, E. Komatsu, H. Tajima, *Physica B-Condensed Matter* **2003**, *329*, 862.
[112] A. Mills, S. LeHunte, *Journal of Photochemistry and Photobiology a-Chemistry* **1997**, *108*, 1.
[113] S. M. Nie, S. R. Emery, *Science* **1997**, *275*, 1102.
[114] C. E. Talley, J. B. Jackson, C. Oubre, N. K. Grady, C. W. Hollars, S. M. Lane, T. R. Huser, P. Nordlander, N. J. Halas, *Nano Letters* **2005**, *5*, 1569.
[115] M. B. Wabuyele, F. Yan, G. D. Griffin, T. Vo-Dinh, *Review of Scientific Instruments* **2005**, *76*.
[116] T. Vo-Dinh, F. Yan, M. B. Wabuyele, *Journal of Raman Spectroscopy* **2005**, *36*, 640.
[117] S. P. Mulvaney, M. D. Musick, C. D. Keating, M. J. Natan, *Langmuir* **2003**, *19*, 4784.
[118] W. E. Doering, S. M. Nie, *Journal of Physical Chemistry B* **2002**, *106*, 311.
[119] K. Kneipp, A. S. Haka, H. Kneipp, K. Badizadegan, N. Yoshizawa, C. Boone, K. E. Shafer-Peltier, J. T. Motz, R. R. Dasari, M. S. Feld, *Applied Spectroscopy* **2002**, *56*, 150.
[120] W. E. Doering, S. M. Nie, *Analytical Chemistry* **2003**, *75*, 6171.
[121] G. C. Schatz, M. A. Young, R. P. Van Duyne, in *Surface-Enhanced Raman Scattering: Physics and Applications, Vol. 103*, **2006**, pp. 19.
[122] M. Moskovits, *Journal of Raman Spectroscopy* **2005**, *36*, 485.
[123] H. G. Li, B. M. Cullum, *Applied Spectroscopy* **2005**, *59*, 410.
[124] A. Otto, I. Mrozek, H. Grabhorn, W. Akemann, *Journal of Physics-Condensed Matter* **1992**, *4*, 1143.
[125] P. Etchegoin, L. F. Cohen, H. Hartigan, R. J. C. Brown, M. J. T. Milton, J. C. Gallop, *Journal of Chemical Physics* **2003**, *119*, 5281.
[126] W. Gu, H. Choi, K. Kim, *Journal of Physical Chemistry A* **2007**, *111*, 8121.
[127] K. Kneipp, H. Kneipp, *Applied Spectroscopy* **2006**, *60*, 322A.
[128] Y. Maruyama, M. Ishikawa, M. Futamata, *Chemistry Letters* **2001**, 834.
[129] V. M. Shalaev, R. Botet, D. P. Tsai, J. Kovacs, M. Moskovits, *Physica A* **1994**, *207*, 197.
[130] K. Kneipp, H. Kneipp, *Israel Journal of Chemistry* **2006**, *46*, 299.

[131] J. Zhang, Y. Fu, M. H. Chowdhury, J. R. Lakowicz, *Nano Letters* **2007**, *7*, 2101.
[132] M. M. Dvoynenko, J. K. Wang, *Optics Letters* **2007**, *32*, 3552.
[133] G. Chumanov, S. Malynych, *International Quantum Electronics Conference (IQEC) (IEEE Cat. No.04CH37598)|International Quantum Electronics Conference (IQEC) (IEEE Cat. No.04CH37598)* **2004**, 2 pp.|1500.
[134] F. J. Adrian, *Journal of Chemical Physics* **1982**, *77*, 5302.
[135] D. D. Evanoff, G. Chumanov, *Abstracts of Papers of the American Chemical Society* **2004**, *228*, U462.
[136] A. Barhoumi, D. Zhang, F. Tam, N. J. Halas, *Journal of the American Chemical Society* **2008**, *130*, 5523.
[137] F. Ni, R. S. Sheng, T. M. Cotton, *Analytical Chemistry* **1990**, *62*, 1958.
[138] T. Vo-Dinh, *Ieee Journal of Selected Topics in Quantum Electronics* **2008**, *14*, 198.
[139] I. H. Chou, M. Benford, H. T. Beier, G. L. Cote, M. Wang, N. Jing, J. Kameoka, T. A. Good, *Nano Letters* **2008**, *8*, 1729.
[140] R. M. Jarvis, R. Goodacre, *Chemical Society Reviews* **2008**, *37*, 931.
[141] W. F. Pearman, A. W. Fountain, *Applied Spectroscopy* **2006**, *60*, 356.
[142] M. J. Banholzer, J. E. Millstone, L. D. Qin, C. A. Mirkin, *Chemical Society Reviews* **2008**, *37*, 885.
[143] R. J. Stokes, E. McBride, C. G. Wilson, J. M. Girkin, W. E. Smith, D. Graham, *Applied Spectroscopy* **2008**, *62*, 371.
[144] D. Lee, S. Lee, G. H. Seong, J. Choo, E. K. Lee, D. G. Gweon, *Applied Spectroscopy* **2006**, *60*, 373.
[145] C. McLaughlin, D. MacMillan, C. McCardle, W. E. Smith, *Analytical Chemistry* **2002**, *74*, 3160.
[146] L. X. Chen, J. B. Choo, *Electrophoresis* **2008**, *29*, 1815.
[147] J. C. Hulteen, R. P. Vanduyne, *Journal of Vacuum Science & Technology a-Vacuum Surfaces and Films* **1995**, *13*, 1553.
[148] A. J. Haes, L. Chang, W. L. Klein, R. P. Van Duyne, *Journal of the American Chemical Society* **2005**, *127*, 2264.
[149] A. J. Haes, C. L. Haynes, A. D. McFarland, G. C. Schatz, R. R. Van Duyne, S. L. Zou, *Mrs Bulletin* **2005**, *30*, 368.
[150] X. Y. Zhang, J. Zhao, A. V. Whitney, J. W. Elam, R. P. Van Duyne, *Journal of the American Chemical Society* **2006**, *128*, 10304.
[151] M. Abdelsalam, P. N. Bartlett, A. E. Russell, J. J. Baumberg, E. J. Calvo, N. G. Tognalli, A. Fainstein, *Langmuir* **2008**, *24*, 7018.
[152] W. E. Smith, *Chemical Society Reviews* **2008**, *37*, 955.
[153] S. E. J. Bell, J. N. Mackle, N. M. S. Sirimuthu, *Analyst* **2005**, *130*, 545.
[154] B. S. Yeo, T. Schmid, W. H. Zhang, R. Zenobi, *Applied Spectroscopy* **2008**, *62*, 708.
[155] M. D. Porter, R. J. Lipert, L. M. Siperko, G. Wang, R. Narayanana, *Chemical Society Reviews* **2008**, *37*, 1001.

[156] S. Keren, C. Zavaleta, Z. Cheng, A. de la Zerda, O. Gheysens, S. S. Gambhir, *Proceedings of the National Academy of Sciences of the United States of America* **2008**, *105*, 5844.
[157] H. W. Tang, X. B. Yang, J. Kirkham, D. A. Smith, *Analytical Chemistry* **2007**, *79*, 3646.
[158] F. Adar, S. FitzeGerald, S. Morel, A. Whitley, *Biophotonic* **2006**, *13*.
[159] X. J. Liu, S. Y. Huan, Y. L. Bu, G. L. Shen, R. Q. Yu, *Talanta* **2008**, *75*, 797.
[160] T. Li, L. P. Guo, Z. X. Wang, *Biosensors & Bioelectronics* **2008**, *23*, 1125.
[161] G. Sabatte, R. Keir, M. Lawlor, M. Black, D. Graham, W. E. Smith, *Analytical Chemistry* **2008**, *80*, 2351.
[162] X. X. Han, L. J. Cai, J. Guo, C. X. Wang, W. D. Ruan, W. Y. Han, W. Q. Xu, B. Zhao, Y. Ozaki, *Analytical Chemistry* **2008**, *80*, 3020.
[163] P. B. Monaghan, K. M. McCarney, A. Ricketts, R. E. Littleford, F. Docherty, W. E. Smith, D. Graham, J. M. Cooper, *Analytical Chemistry* **2007**, *79*, 2844.
[164] C. Budich, U. Neugebauer, J. Popp, V. Deckert, *Journal of Microscopy-Oxford* **2008**, *229*, 533.
[165] B. S. Yeo, S. Madler, T. Schmid, W. H. Zhang, R. Zenobi, *Journal of Physical Chemistry C* **2008**, *112*, 4867.
[166] K. F. Domke, D. Zhang, B. Pettinger, *Journal of the American Chemical Society* **2007**, *129*, 6708.
[167] E. Bailo, V. Deckert, *Angewandte Chemie-International Edition* **2008**, *47*, 1658.
[168] T. Schmid, A. Messmer, B. S. Yeo, W. H. Zhang, R. Zenobi, *Analytical and Bioanalytical Chemistry* **2008**, *391*, 1907.
[169] E. Bailo, V. Deckert, *Chemical Society Reviews* **2008**, *37*, 921.
[170] R. M. Jarvis, A. Brooker, R. Goodacre, *Faraday Discussions* **2006**, *132*, 281.
[171] T. Moehring, M. Kellmann, M. Jurgens, M. Schrader, *Journal of Mass Spectrometry* **2005**, *40*, 214.
[172] J. Garcia-Hernandez, L. Cadena-Cardenas, M. Betancourt-Lozano, L. M. Garcia-De-La-Parra, L. Garcia-Rico, F. Marquez-Farias, *Toxicological and Environmental Chemistry* **2007**, *89*, 507.
[173] S. Seitz, C. K. Schneider, J. Malotka, X. Nong, A. G. Engel, H. Wekerle, R. Hohifeld, K. Dornmair, *Proceedings of the National Academy of Sciences of the United States of America* **2006**, *103*, 12057.
[174] B. V. Safronov, V. Pinto, V. A. Derkach, *Journal of Neuroscience Methods* **2007**, *164*, 292.
[175] L. A. Sklar, B. S. Edwards, S. W. Graves, J. P. Nolan, E. R. Prossnitz, *Annual Review of Biophysics and Biomolecular Structure* **2002**, *31*, 97.
[176] M. Qin, S. Hou, L. K. Wang, X. Z. Feng, R. Wang, Y. B. Yang, C. Wang, L. Yu, B. Shao, M. Q. Qiao, *Colloids and Surfaces B-Biointerfaces* **2007**, *60*, 243.